UNIVERSITY OF GAZIANTEP
GRADUATE SCHOOL OF
NATURAL AND APPLIED SCIENCES

EARLY AGE TEMPERATURE DISTRIBUTIONS IN
REINFORCED CONCRETE BOX GIRDER

M.Sc. THESIS
IN
CIVIL ENGINEERING

BY
HASSAN HASHIM ATIYA
DECEMBER 2014

Early Age Temperature Distributions in Reinforced Concrete Box Girder

M.Sc. Thesis
In
Civil Engineering
University of Gaziantep

Supervisor
Assist. Prof. Dr. Nildem TAYŞI
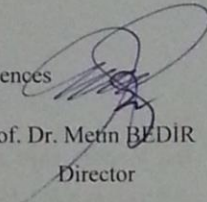
By
Hassan Hashim ATIYA
December 2014

REPUBLIC OF TURKEY
UNIVERSITY OF GAZİANTEP
GRADUATE SCHOOL OF NATURAL AND APPLIED SCIENCES
CIVIL ENGINEERING

Name of the thesis: Early Age Temperature Distributions in Reinforced Concrete
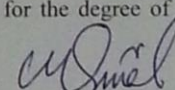Box Girder.

Name of the student: Hassan Hashim ATIYA
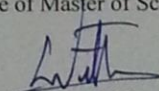
Exam date: December 3, 2014

Approval of the Graduate School of Natural and Applied Sciences

Prof. Dr. Metin BEDİR

Director

I certify that this thesis satisfies all the requirements as a thesis for the degree of
Master of Science.

Prof. Dr. Mustafa GÜNAL

Head of Department

This is to certify that we have read this thesis and that in our consensus opinion, it is
fully adequate, in scope and quality, as a thesis for the degree of Master of Science.
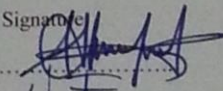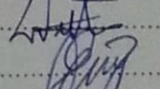
Assist. Prof. Dr. Nildem TAYŞİ

Supervisor
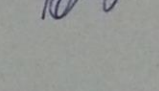
Examining Committee Members   Signature

Prof. Dr. Mustafa ÖZAKÇA

Assist. Prof. Dr. Nildem TAYŞİ

Assoc. prof. Dr. Ahmet ERKLİĞ

Declaration

I hereby declare that all information in this document has been obtained and presented in accordance with academic rules and ethical conduct. I also declare that, as required by these rules and conduct, I have fully cited and referenced all material and results that are not original to this work.

Hassan Hashim ATIYA

ABSTRACT

EARLY AGE TEMPERATURE DISTRIBUTIONS IN REINFORCED
CONCRETE BOX GIRDER

ATIYA, HASSAN HASHIM
M.Sc. in Civil Engineering
Supervisor: Assist. Prof. Dr. Nildem TAYŞI
December 2014
71 pages

The analysis of bridge temperatures during the early age of concrete is a complicated problem. At early ages, cement hydration produces an internal heat, which depends mainly on the chemical composition of cement. This heat is added to the permanent and fluctuated time-dependent heat gained from or lost to the surrounding atmosphere. The effect of the daily temperature change and the seasonal movement of the sun can leads to serious thermal movements or stresses along the span of the bridge. In this research, an experimental program was used to study the temperature distribution in concrete bridge superstructures during the early age of construction. For this aim, a full-scale experimental box-girder bridge segment was constructed in Gaziantep University. Thermocouples were installed in the slabs and the walls to monitor the temperature changes of concrete. Moreover, pyranometer and anemometer were used to record the solar radiation and wind speed, respectively. In addition, a temperature probe with solar radiation shield was installed to monitor the ambient air temperature. The results showed that concrete temperature was mainly related to the location of thermocouples. Interior thermocouples were much influenced by hydration heat, while the temperatures of the near surface thermocouples showed higher dependency on air temperature than on hydration heat. A maximum temperature gradient of approximately 25 ℃ was recorded between the interior and the exterior thermocouples of the south web.

Keywords: air temperature, box-girder, hydration heat, temperature gradient, solar radiation

ÖZET

BETONARME KUTU KİRİŞDEKİ TAZE BETONUN SICAKLIK DAĞILIMI

ATIYA, Hassan Hashim
Yüksek Lisans Tezi, İnşaat Müh. Bölümü
Tez Yöneticisi: Yrd. Doç. Dr. N. TAYŞİ
Aralık 2014
71 sayfa

Köprü betonunun yeni döküldüğü dönemindeki sıcaklık analizi karmaşık bir konudur. Yeni döküldüğü dönemde, çimento kimyasal bileşimlerine bağlı olarak çimento hidratasyonu bir iç ısı üretir. Bu ısı, sabit veya dalgalı olarak zamana bağlı çevredeki atmosferden elde edilen sıcaklığa eklenir. Atmosferdeki bu sürekli ısı değişimi, iklim değişikliği ve günlük ve mevsimlik güneşin hareketi tarafından üretilen hava sıcaklığı, rüzgar hızı ve güneş ışıması gibi termal yükler nedeniyle oluşur. Bu çalışmada, beton köprü süper yapılarında betonun yeni döküldüğü dönemdeki sıcaklık dağılımını incelemek için deneysel bir yöntem kullanılmıştır. Bu amaçla, tam ölçekli bir deneysel kutu kirişli köprü parçaşı Gaziantep Üniversitesi kampüsünde inşa edilmiştir. Beton sıcaklık değişikliklerini gözlemlemek için döşeme ve duvarlara termokapıllar yerleştirilmiştir. Ayrıca, piranometre, solar radyasyon ve anemometre, rüzgar hızını kaydetmek için kullanılmıştır. Ayrıca, güneş ışınım kalkanlı bir sıcaklık ölçer ortam hava sıcaklığını ölçmek için yerleştirilmiştir. Sonuçlar, beton sıcaklığının esas olarak thermokapılların konumu ile ilgili olduğunu göstermektedir. Yüzeye yakın olan termokapıllarda hidratasyon sıcaklığından daha fazla hava sıcaklığı önemli iken, içteki termokupllar, hidratasyon ısısından daha fazla oranda etkilenmektedirler. Güneydeki iç ve dış termokapıllar arasındaki maksimum sıcaklık farkı yaklaşık 25 ℃ olarak kaydedilmiştir.

Anahtar Kelimeler: hava sıcaklığı, kutu kirişler, hidratasyon ısısı, sıcaklık gradyan, güneş ışınımı

ACKNOWLEDGEMENTS

First of all, great thanks to Allah his Majesty for enabling me to complete this work.

I would like to express my respect and regards to my supervisor, Assit. Prof. Dr. Nildem Tayşi, for guidance, advice, encouragement and suggestions during the preparation of this thesis.

My gratitude and appreciation to the my dissertation committee members, especially Prof. Dr. Mustafa ÖZAKÇA and Assist. Prof. Dr. Ahmet ERKLIĞ.

I wish to express my gratitude to the University of Gaziantep, civil engineering department . I will always be grateful for their help in fulfilling my dream

I wish to thank Ph.D student A, R. Sallal for allowing me the time to complete this work. I also wish to thank him for the help, expertise, and encouragement he offered.

I want to thank the other students who I got to know and appreciate. The friendship and help of these many talented individuals helped me immensely, especially Ph.D Abbas, Yahya, Salih, Ihssan.

My special thanks are reserved for my wife for her understanding, patience and great help. My wife supported and encouraged me strongly and consistently through the studying period and enduring some loneliness. Her endless love and support kept me studying.

I cannot express my gratitude enough to my sons, Maryam, Ali and, my sweetheart, my daughter Zahra. They paid the cost of my work and to them I express my love and thanks.

CONTENTS

LIST OF FIGURES

LIST OF TABLES

LIST OF SYMBOLS, ABBREVIATIONS AND NOMENCLATURE

C_3S	Tricalcium Silicate
C_2S	Dicalcium Silicate
C_3A	Tricalcium Aluminate
SO_3	Sulfur Trioxide
ASTM	Standard Test Method
K_x, k_y, k_z	Thermal conductivity in direction x, y, z
q_s	Quantity of heat gain from the sun: solar radiation
$\dot{q}$	Rate of heat generation W/m^3
ρ	The density of the material kg/m^3
c	The specific heat of the material, $KJ/°C . kg$
I	Normal component of solar radiation incident
α	The coefficient of absorption
t	The time
h_c	Convection heat transfer coefficient
T_s	Surface temperature
T_a	Ambient air temperature
q_c	Quantity of heat gain/loss due to the temperature difference between the air and the boundary surface
ε	The emissivity of the surface
σ	Stefan-Boltzmann constant (5.677 x 10^{-8}) $W/m^2. K^4$
T_s	The temperature of the surface
T_a	Ambient air temperature
T	Temperature
k	Thermal conductivity coefficient
FETAB	Finite Element Thermal Analysis of Bridges
CBGB	Concrete Box Girder Bridge
2D	Two dimensional
3D	Three dimensional
°C	Temperature scale, Celsius

AASHTO	American Association of State Highway and Transportation Officials
ANSYS	Finite Element Program
FE	Finite Element
ACI	American concrete institute
BS	British standards code
E-W	East-West
DINI. 072.	Road and Foot Bridges Design Loads, Deutsche institute Normung, Berlin
a.m.	before midday
p.m.	after midday

CHAPTER 1

INTRODUCTION

1.1 General

The Box girder bridges are subject to different loading such as dead loads, live loads and environmental loads. The environmental loads are complicated to account for the design of the bridges. With the development of technology in the last years, bridge construction technology evolved sufficiently to consider loads such as thermal loads, wind, earthquakes, etc. Bridge structures are exposed to the atmospheric conditions and subjected to solar radiation, air temperature and wind speed. The intensity of solar radiation depends upon the clearance of the atmosphere and the relative position of the sun. The bridge surfaces are gained heat by radiation or convection and then dissipated to the interiors of the bridge by heat conduction process. However, and after nightfall, when the source of heat does not exit, the bridge itself becomes a source of radiation and loses heat by convection to the surrounding air.

Studies on thermal loads in different box girder bridges subjected to change of environmental conditions had been conducted all over the world. The previous researchers roughly divided these studies into three categories; theoretical, numerical and field measurements. The theoretical methods use solutions of the heat transfer equation and detect the temperature distribution in bridges, which must employ a series of assumptions. The numerical methods utilized numerical solutions of the heat equation such as the finite element method or finite difference method, which can give appropriate measurements if the input parameters are checked properly. The field measurements get the temperature distribution by the temperature sensors that installed inside the concrete to monitor the temperature changes of concrete in different position of the bridge.

Because of the structural advantages of tensional stiffness, box girder bridges have become a popular solution for medium and long span bridges and are increasingly constructed for modern highways. Due to this importance, further researches are required to understand the behavior of box girder bridges under the different types of loading. Among these loadings, thermal loads can play an important role and can cause stresses and deformations that affect the long-term durability and hence the structural integrity of the bridge girders.

When concrete is cast in the field, the fluctuation of temperature inside and on the surfaces of the different parts of the bridge girders is very complicated. The complexity of this problem comes from the individual complexities of the different thermal loads affecting the concrete girder. Due to their continuous external exposure, bridge girder surfaces are subjected to the ambient air temperature in addition to the solar radiation heating loads. In addition, wind speed can be considered as an effective cooling load.

During the early ages, the internal heat produced by cement hydration is added to the previous external thermal loads. Each of the previous thermal loads depends on many factors, some of which are environmental factors and some are chemical factors. Some of which are time dependent, while others are not. The relations that correlate these thermal loads with the affecting factors are linear in some cases like the convective cooling and nonlinear in others like the surface-to-ambient radiation. Consequently, the combination of the different thermal loads leads to temperature gradients both vertically and laterally. Thus, leads to thermal strains and hence stresses or deformations within the depth and the width of the girder section and longitudinally along the bridge span.

Temperature measurements for the first five days from concrete casting of an experimental box girder segment were used and analyzed in this study to investigate the combined effect of the hydration heat and the environmental thermal loads on the distribution of temperature in box girder bridges during the early age of concrete.

1.2 Objective of the Study

Temperature data from an experimental box girder segment was analyzed in this study to investigate the temperature variations within concrete box girder bridges during the early few days of the age of concrete.

The objectives of the current study are:

- Investigating the time dependent temperature variations of concrete due to the combined effect of the environmental thermal loads and the hydration heat during the early age of the concrete at different parts of the girder section. The investigated thermal loads include the solar radiation, the temperature of the ambient air and the speed of the wind.

- Studying the vertical and the lateral temperature distributions along the webs and the flanges of the girder at different times from concrete casting up to five days later.

- Studying the effect of hydration heat on the vertical and the lateral temperature gradients along the webs and the top and bottom flanges of the girder during the early age of concrete.

1.3 Layout of the Thesis

This thesis composed of five chapters; the first chapter gives a brief introduction about the studied subjects, which are the effect of environmental thermal loads on concrete bridges and the hydration of cement and its effect during the early age of concrete.

In chapter two, the hydration process of cement is discussed in more details mentioning the effective factors and methods of measurements. Moreover, the heat conduction in concrete and the environmental thermal loads affecting the boundary surfaces of concrete bridges are also discussed in more details in chapter two. Finally, in chapter two, study details and methods of measurements and solutions in addition to the important results of many previous studies are reviewed.

Chapter three discusses the temperature measurements in the experimental concrete box girder segment and reviews the type and the distribution of sensors used for this

purpose. In chapter four, the temperature variations, distributions and gradients are discussed for the early age of concrete, which is limited with the first five days from the age of concrete. Finally, chapter five lists the most important conclusions from the discussion of the experimental results.

CHAPTER 2

LITERATURE REVIEW

2.1 Introduction

Temperature affects the conduct of early age concrete in many ways. It affects the cement hydration, shrinkage and creep, and it generates stresses and cracking in concrete structures. The temperature distribution in hardening concrete change with time as a consequence of environmental variations and particularly, the cement hydration. The important temperature variations due to heat of hydration can be predictable in massive concrete members at an early age. The factors affecting the temperature rise in concrete due to hydration heat and other heat sources such as solar radiation are complicated, because the temperature distribution changes in space and time and boundary conditions.

Therefore, temperature distribution is a very important to both the designers and contractors of the concrete bridges. At an early age the box girder bridge subjected to environmental conditions such as the solar radiation, the ambient air temperature, and the wind speed and in addition to the heat generated by cement hydration. This chapter includes three sections, the first one brief description of the heat of hydration and the factors that affects of cement hydration. The second one discusses the effect of environment thermal loads on concrete bridges, and the last section, a summary of research that has been done in the field of temperature distribution and thermal gradients in the concrete box girder bridges.

2.2 The Heat of Hydration in Concrete

The amount of liberated heat from the hydration of cement depends upon the physical properties and chemical components of the manufacture cement. As shown in Figure 2.1, the whole process of cement hydration was divided into five stages. Stage 1: when cement is mixed with water, the reaction occurs and rapid heat evolution, because ions resolving in the water and interact with C_3A and gypsum.

The period of stage 1 about fifteen to thirty minutes, therefore it has a small impact on strength of concrete.

Stage 2: little heat was produced, because the cement hydration ceases, the concentration of ions Tricalcium Silicate (C_3S) and Dicalcium Silicate (C_2S) increases in the concrete system, it is important during the mixing, transporting, workability and placing of the concrete. This period continues less than five hours. This stage is known as dormant period.

Stage 3: (the acceleration period), the compounds (C_3S) and (C_2S) start again to release heat, therefore concrete temperature rises rapidly and usually heat liberation. In this period, strength is developed and early hardening in concrete has begun so, stage3 is more important to knowledge the characteristic of concrete.

Stage 4: (the deceleration period), while the time increases, heat generation gradually decreases, thickness of hydrated layers increases, the diffusion area that gives water permeability and dissolved ions.

Stage 5: (the steady state period), finally, the cement hydration reaches steady state and stages 4 and 5 are called as a diffusion control phase. Figure 2.1 shows the hydration process.
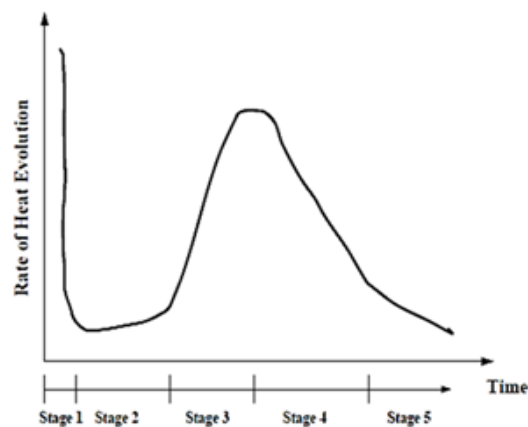
Figure 2.1 The heat of the hydration process [1]

2.3 The Factors Effect on the Hydration Heat [1]

The amount and rate of the liberated heat was depended upon the chemical and physical properties of the cement. The factors are explained the following section:

2.3.1 The type of cement

The heat liberation for kinds of manufacturing cement under similar circumstances was very important. Lerch and Ford [2] and the Danish Concrete Association [3] tested that cement type 3 liberates heat 3-5% more than cement type 1. The various in the emitted heat from the different kinds of cement is mainly due to the cement fineness and the chemical composition

2.3.2 The chemical composition of cement

The effect of chemical composition depends upon the amount of heat liberated and it is a percentage in the cement. Lerch and Bough [4]   found that when increasing the Tricalcium Aluminate C_3A content to 20%, the heat generation increases to about 50%, but the effect of C_3A compound is steady after sixteen hours regardless the C_3A content.

2.3.3 The content of sulfate

Lerch [5]   found that when increasing the percentage of the Sulfur Trioxide (SO_3) the heat liberated was decreased in 30 minutes with regardless of the amount of content of Tricalcium Aluminate (C_3A).

2.3.4 Fineness

The effect of fineness of cement improvement the moisture content and workability of concrete mixture.

2.3.5 Water cement ratio

Z. Qian et al [6] studied three different water / cement ratios, 0.3, 0.4, and 0.5 respectively, and they found that the almost 0.4 was required percentage to continue the hydration cement complete and the degree of hydration was decreased and stop when the water cement ratio was 0.3 as well as the other cases (water / cement ratio 0.4 and 0.5) the tensile strength will increase when the cement hydration increase.

2.3.6 Curing and initial temperature

The heat of hydration was increasing under high temperature on hot days and it was decreased with time. Early exposure of concrete to high temperature will be reduce the concrete strength at a later age.

2.3.7 The chemical mixture

The chemical mixture is used to improve the time of mixing and reduce the required water of the concrete. ASTM C 494 [7] classified the chemical admixture to about seven types.

2.3.8 Existing test methods

There are four methods used to measure the heat of hydration of cement [8].

- The adiabatic calorimeter.
- The semi-adiabatic calorimeter.
- The isothermal calorimeter.
- The solution calorimeter by using a standard test method ASTM C186.

2.4 The Effects of Environmental Thermal Loads on Concrete Bridges

The temperature distribution within a structure or the boundaries of a structure as the heat flux are represented by the following equation [9].

$$\frac{\partial}{\partial x}\left(k_x \frac{\partial T}{\partial x}\right) + \frac{\partial}{\partial y}\left(k_y \frac{\partial T}{\partial y}\right) + \frac{\partial}{\partial z}\left(k_z \frac{\partial T}{\partial z}\right) + \dot{q} = \rho c \frac{\partial T}{\partial t} \qquad (2.1)$$

T is temperature°C

k_x , k_y ,k_z is thermal conductivity in direction x, y, z

$\dot{q}$ is rate of heat generation W/m^3

ρ is the density of the material kg/m^3

c is the specific heat of the material, $KJ/°C . kg$

The heat generated within a structure is the cement hydration.

2.4.1 Components of boundary heat flow

The boundary conditions of heat transfer of concrete bridge in the environment consists such as, the convection, solar radiation, and thermal irradiation. Figure 2.2 shows that the components of the boundary heat flow of the concrete.
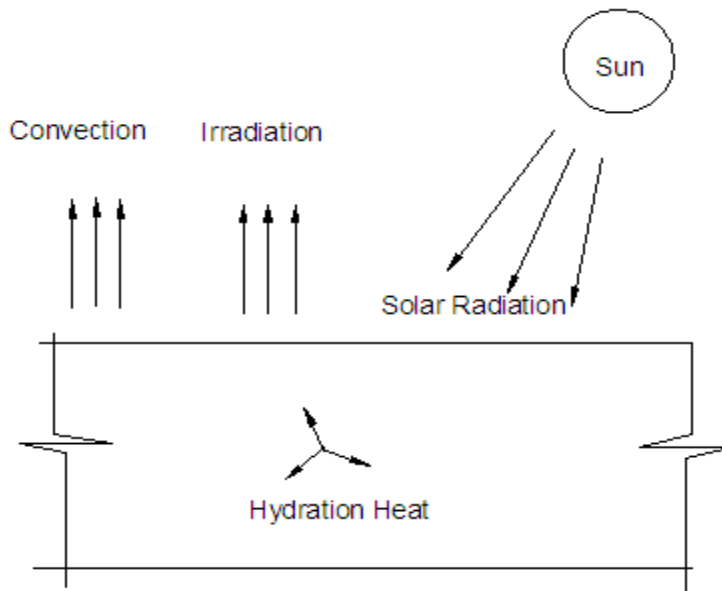
Figure 2.2 The natural boundary condition of concrete

2.4.2 Solar radiation intensity

The solar radiation heat flux is affected by many factors, and it can be calculated from the assumed parameters of the atmosphere, the time of day, the date of the year and the others.

Kreith [10], Duffie and Beckman [11] discovered procedure to measure the solar radiation on a surface from parameters, like geometry, geographical location, the turbidity factor and the mass factor. The computation purpose is affected by the turbidity and the air mass factors. The turbidity factor defines the ratio of the attention to the average molecular scattering coefficient. It is valued about 2.0 to 5.0, very clear air and very smoky respectively [9]. The solar radiation received by the structures and can be calculated by the following function [9].

$$q_s(t) = \alpha \, I(t) \qquad\qquad (2.2)$$

Where I is a normal component of solar radiation incident on the surface of the structure

α is the coefficient of absorption

t is time

Then I depends on the clearness of the atmosphere and the relative position of the sun

2.4.3 Convection heat transfer

The convection heat transfer occurs between the surfaces of a structure and the ambient air temperature as a result of the temperature difference between them. The convection heat transfer is represented by classic Newton's law of cooling [9].

$$q_c(t) = h_c[T_S(t) - T_a(t)] \tag{2.3}$$

Where, h_c is convection heat transfer coefficient

T_s is surface temperature

T_a is ambient air temperature

t is time

For structures, outdoor the h_c depends on the wind speed and the surface roughness. The estimation of the value for h_c is sometimes very difficult in the structures and there is always a probable of about 25 % error [9].

Billington [12] assumed that the relation between h_c and wind speed was linear. Emerson [13] found that then h_c on the bottom surface of the bridge was almost half of the top surface

2.4.4 Thermal irradiation

The heat transfer between the surfaces and objects or ambient air of the structures can be expressed through the Stefan – Boltzmann law [9]. The emissivity of thermal irradiation and the absorption of solar radiation are sometimes different because the big temperature difference between the sun and a body on the earth [9]

$$q_r(t) = \varepsilon\sigma[T_s^4(t) - T_a^4(t)] \tag{2.4}$$

Where, σ is the Stefan-Boltzmann constant (5.677 x 10^{-8}) $W/m^2 . K^4$

ε is the emissivity of the surface

T_s is the temperature of the surface

T_a is the temperature of the air

2.4.5 Ambient air temperature

The difference of the ambient air temperature depends upon the protection and location of the structure and also environmental conditions, on the special case, at inside a regulated environment, the ambient air temperature is constant. However, most cases the air temperature is assumed between the maximum and minimum temperatures. The computer program (FETAB) can also use to be calculated the air temperature. Hursley [14], Dilger and Ghali [15], gave detailed procedures for a calculation the ambient air temperature

2.5 The Main Types of The Formwork

There are important types of materials used as formwork in structures of concrete, namely, wood and steel. The thermal conductivity (k) of the two types of materials is different, where the value of the 40 - 50 $W/m.°C$ and $0.1 - 0.15 \ W/m.°C$ for steel and wood, respectively [9].

The influence of steel formwork on thermal changes in concrete is neglected for large structures, that is, the effects of steel formwork can be negligent in the thermal analysis of concrete structures.

In addition, the thermal conductivity of wood is very low, therefore the wood formwork is a good heat insulator to keep the concrete from the environmental conditions and to reduce the temperature gradient in the cross section.

When the concrete subjected to the cold environment at an early age due to the insulation removed will cause a rapid drop in temperature near surface, therefore it leads to thermal cracking on the concrete surface.

2.6 Previous Studies

There have been many studies of temperature distribution measurements in full scale models of the concrete box girder, which are subjected to environmental thermal loads. The early researchers on the thermal effects of concrete started in the early fifties of the twentieth century, where the research was based on the heat transfer in

one dimensional in the vertical direction depending on the experimental information or empirical formulas.

Many researchers have been conducting studies on the temperature behavior of highway bridges. The researcher concluded that the thermal loads were influenced by the intensity of the solar radiation, air temperature material type and wind speed after the investigation on many bridges.

Zuk [16] developed a method for calculating thermal stresses and deflections from linear thermal gradients in composite steel bridges.

Zuk [17] tried to predict the maximum temperature of the surface of a composite steel bridge in Virginia, as well as he suggested empirical formula for the measurement of the maximum vertical temperature gradient between the top and the bottom of the composite bridge.

Emerson [18] conducted many field measurements on concrete, steel and composite bridges of different cross sections located in Wales and England, continued this research until 1982. Emerson noted that the temperature gradients in the bridge were not various from those measured in the previous years. Emerson concluded that the large positive and the large negative temperature gradient can occur at least five times a year. Emerson carried out a series of tests to investigate the effect of the thickness of surfacing on maximum temperature gradients in six different depths of the differential cross section in the bridge structure. Table 2.1   shows that the influence of the thickness on the temperature gradients in bridges in the United Kingdom.

Table 2.1 Temperature gradients in bridge in the United Kingdom [18]

Bridge structure	Type	Depth (m)	Thickness (mm)	T (℃)	T(℉)
Adur	CBGB	1.1	64	17.0	62.6
Coldra	I-Beam	1.14	102	13.0	55.4
Mancunian	CBGB	1.3	90	14.0	57.2
Hammersmith	CBGB	2.0-2.7	92	15	59.0
Medway	I-Beam	2.4-2.7	57	16.0	60.8
MarlowBishom	CBGB	1.52- 4.15	150	17.0	62.6

CBGB is the Concrete Box Girder Bridge

Maher [19] suggested a linear temperature distribution for concrete box girder sections, according to experimental studies in the United Kingdom and Australia. He proposed variation through the flange section, he thought that the desk slab of the bridge was the most important. Temperature distribution is shown in Figure 2.3.

25 ℃

Bottom surface of top Slab
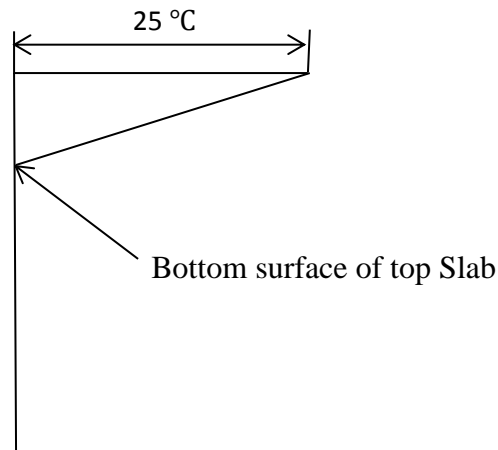
Figure 2.3 Temperature distribution suggested by Maher [19]

Emerson [20] modified a one- dimensional finite difference model to measure temperature distribution in concrete, steel and composite bridges due to ambient air temperature, wind speed and solar radiation effects. Emerson considered the calculation of temperature distributions started at 8 am and 4 pm in the summer and winter, respectively. The reversed temperature gradients were happened at 6±1 am for box section and thick slab and 5±1 am for thin slab in winter, the maximum

temperature gradients were happened at 4±1 pm for the box section thick slab and 3±1 pm for thin slab in summer.

Will et al. [21] conducted a 2D finite element program for predicting the internal temperature distribution and thermal stresses of concrete bridges. The 2D finite element program analysis used to estimate the thermal stresses for the bridges, and the result obtained from the analytical procedures closely connected with the field measurements.

Priestly [22] suggested the temperature gradient to a fifth power curve from the top surface down to a maximum height of 1.2 m which is appropriate for T- beam, slabs cantilever and web of concrete box girder sections. In addition, a linear temperature distribution along the both 0.2 depths of the section.

For concrete depth of an enclosed air cells of the above, a linear temperature gradient is specified to explain the insulating effect of the air cell. The vertical temperature gradient suggested by Priestly is shown in Figure 2.4. Priestley considered that this revised temperature gradient would lead to an essential decrease in the tension stress.

$$T(y) = T_{top}(1200/y)^5$$
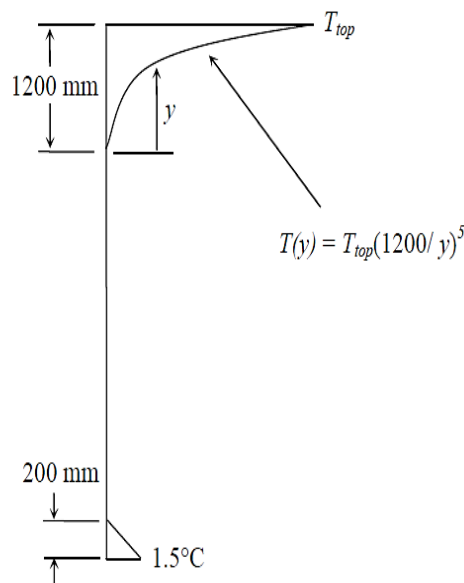
Figure 2.4 Vertical temperature gradient proposed by Priestley [22]

Degenkolb [23] summarize 30 years of experience in the design and construction the box girder bridge. Degenkolb summarize many designs and noted that the transverse temperature gradients more significant than the thermal gradient through the depth. Thermal gradient through the depth caused forces and rotations and may be decreased by rotating bearings and expansion joints. However, the transverse temperature gradients may be caused longitudinal cracking in the webs of the box girder. The air temperature outside the box can be different from the inside air temperature, therefore the temperature distribution across the webs may be different from one side to another on the bridge. Degenkolb recommends minimizing the transverse temperature stresses by using thin girder webs to increase their flexibility and decrease stress

Hambly [24] offered a simplified method to compute the temperature distribution through the cross section of the concrete box girder. He explained that the inside air temperature of the concrete box cell differs approximately 1 to 2 on the day. Therefore, in the design it is appropriate to assume that constant during the day.

Emanuel and Hulsey [25] used the finite element method to predict maximum temperature and minimum temperature of bridge deck and vertical temperature gradient in composite bridges exposed to environmental conditions of Mid- Missouri. The observed measurements explained that the maximum and minimum temperature of bridge deck were about 66 ℃ and 23 ℃ for summer and winter respectively, and the vertical temperature gradient between the top and bottom were 22 ℃ and 17 ℃ respectively

Wood [26] carried out a field study on five pre-stressed concrete bridges in Newzland for approximately four years. The researcher noted that the observed largest temperature gradients were 22.3 ℃ between the top and the bottom surfaces at 4 pm for 1.68 m box girder with 40 mm of surfacing, and the researcher concluded that the steep thermal gradient was possible four or five times a year.

Wanders [27] carried out a field study on the temperature measurements of the Turkey Run bridge, located in Indiana, USA. The period of the study was one year, recorded The highest positive temperature gradient was 13.5 ℃ in 26 June and the highest negative temperature was – 4 ℃ in 27 February.

Dilger et al. [28] observed the thermal behavior a concrete and steel composite bridge during the casting of the concrete deck and continue for 3 years. The results showed that, there were cracks in the concrete deck and nonlinear strain distributions developed across the depth. Furthermore, they recorded rapid heating of steel boxes exposed direct sunlight

Hoffmann et al. [29] reviewed the results of temperature distribution recorded in the summer of 1979 on a pre-stressed box girder located at the Pennsylvania from the Transportation Research Facility. The maximum surface temperature gradient was 10.5 ℃ which, is near to the New Zealand recommendation of 14.2 ℃.

Elbadry and Ghali [30] conducted a parametric study of the influence of bridge orientation surface conditions, the climatic conditions, the girder geometry on temperature distributions and thermal stresses of bridges, using a 2D finite element program. Based on to the study, the combination of surface and environmental conditions are controlling the temperature distribution and stresses in the concrete box girder.

Elbadry and Ghali [31] investigated concrete cracks and tensile stresses caused by the nonlinear temperature distribution in the bridges and offered a lower quantity of reinforcements to reduce the width of temperature cracks.

Mirambell and Aguado [32] proposed 2D finite difference methods to calculate stress and temperature distributions in box girder bridges. In this study, the researchers confirmed the impact of the transverse temperature gradients between external air and the air inside the concrete box which can induce tensile stresses at the inside or outside of the web and slab in the concrete box girder.

Moorty and Roeder [33] utilized the finite element method to study the temperature response of composite bridge exposed to the external environmental conditions. The steel girder was modeled using 3D beam element and the concrete deck was modeled using plate elements. The temperature distributions and the thermal conduction gained from the analytical models were compared with the measurements for verifying the proposed model. The study also examines the effect of various bridge's geometries and the thermal response in the composite bridges.

Gilland and Dilger [34] measured temperature changes, ambient air temperature, wind speed and solar radiation during the construction of a pre-stressed box girder located in Atlantic, Canada. The temperature of fresh concrete was gradually raised due to cement hydration. After the formwork was taken away, the thermal gradient increased dramatically, due to the surrounding environmental conditions of the bridge.

Wollman et al. [35] compared the results of concrete temperature obtained by a field study on a segmental box girder in San Antonio, Texas with the recommendations of the AASHTO LRFD Bridge Design Specifications (1994) and the AASHTO Segmental Specifications (1999). For the positive thermal gradient measured in this study, the AASHTO LRFD (1994) offered the highest vertical gradients for the surface without surfacing. The AASHTO (1999) showed highest vertical gradients for positive and negative thermal gradient. Moreover, this study suggested the relationships between the measured temperature of concrete box girder and the ambient environmental conditions for predicting positive thermal gradients.

Pisani [36] observed the influence of nonlinear thermal strain induced by daily and seasonal variation in environmental effects in pre-stressed concrete decks and in reinforcements. The results showed that the thermal impacts did not significantly influence the load capacity, but affected the strains and stresses of concrete box girder under service loads.

Zhang et al. [37] conducted a numerical study of temperature field of concrete box girder depends on the temperature analysis between field temperature and numerical simulation of temperature field based on the heat exchange equilibrium theory of pre-stressed concrete box girder. The study shows that the temperature field numerical simulation was reflected high accuracy of actual boundary conditions and able to meet the design and analysis, practical, in addition the calculation programs of temperature field for concrete box girder based on the ANSYS program had more features, like simple operation and the possibility to delete some repetitive tasks.

AASHTO LRFD bridge design specification [38] divided the United States into four solar radiation zones. Section 3.12.3 and as shown in table 2.2 provided the temperature gradients in the concrete structures. The vertical temperature gradient in

concrete and steel structures is shown in Figure 2.5. The dimension A in Figure 2.5 shall be taken as 30 cm for the concrete structures which are 40 cm or more than in depth, and 10 cm for the concrete structures was less than 40 cm in depth. For steel structures dimension A equal to 30 cm, and t was the depth of the concrete deck . The temperature value T_3 shall be taken as 0 ℃, unless a site-specific study is made to determine an appropriate value, but it shall not exceed 2.8 ℃.

Table 2.2   The temperature gradients in concrete [38]

Zone	T_1 (℃)	T_2 (℃)
1	30	7.7
2	25.5	6.6
3	22.7	6.1
4	21.1	5
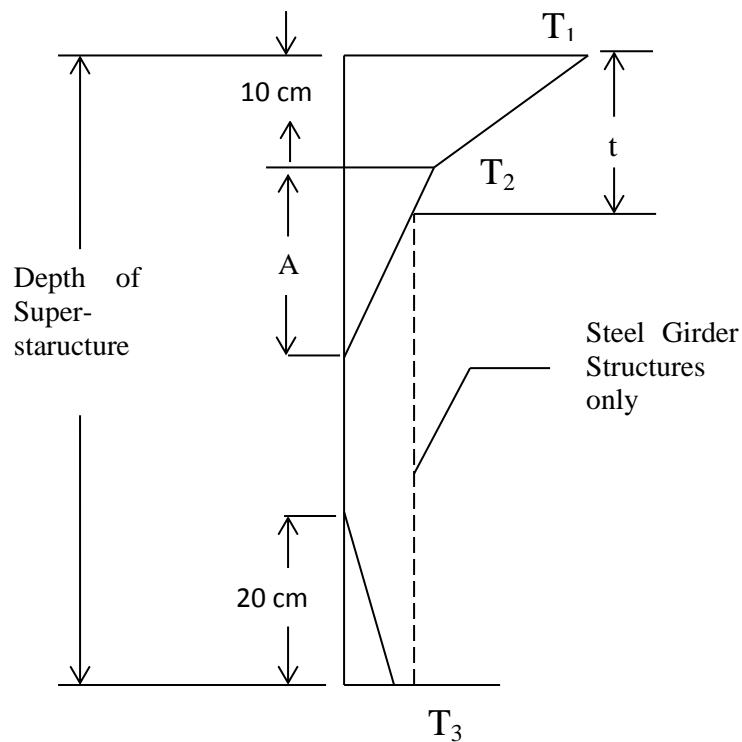
Figure 2.5 The vertical temperature gradient in concrete and steel structures [38]

Gu Bin et al. [39] carried out field studies on the effect of cold wave on the temperature gradient in concrete box girder bridge. They utilized temperature sensors, anemometer, humidity sensors and strain gauges to measure the effect of the cold wave on the concrete box girder bridge. The researchers proposed two dimensional model to predict the temperature gradient across the section of the box girder bridge. They concluded that the temperature distribution under the environmental conditions (solar radiation, air temperature cooling) were various about the effect of cold wave on the concrete box girder, and temperature low due to the cold wave may cause more difficult to the concrete, especially the large concrete box girder.

Also, they found that the temperature distribution across the section of the box girder due to the influence of cold wave is not similar the effect of the environmental conditions like solar radiation and cooling load during the night, and they proposed two dimensional temperature gradient model to investigate the purpose this study.

In 1989 AASHTO Guide Specifications [40], depended on the National Cooperative Highway Research Program Report 276, also provided variation temperature distributions and uniform bridge temperatures as well published the AASHTO GS, thermal influences in concrete bridge superstructures in 1989 for the bridge superstructures and design of reinforced. The uniform bridge temperatures, which produces in the contraction and expansion of bridge superstructures, were termed effectiveness bridge temperatures in the AASHTO GS.

The guidelines of the AASHTO GS supplied the values of minimum and maximum effectiveness bridge temperatures depended on minimum and maximum normal air temperatures at the site of the bridge. Table 2.3 shows the temperatures interconnected the actual daily air temperatures for the concrete bridges. The profile and the values of the vertical thermal gradients from the AASHTO GS are shown in Figure 2.6 and Table 2.4.

Table 2.3 Correlation between the normal daily air temperatures and effective bridge temperatures [40]

Normal Daily Minimum Temperature, (^{o}C)	Minimum Effective Bridge Temperature, (^{o}C)	Normal Daily Minimum Temperature, (^{o}C)	Minimum Effective Bridge Temperature, (^{o}C)
-34.4	-19.4		
-31.6	-17.7	12.7	18.8
-28.6	-16.2	15.5	20.5
-26.1	-15.1	18.3	22.7
-23.3	-13.3	21.1	24.9
-20.5	-11.6	23.8	26.6
-17.7	-10.5	26.6	28.8
-14.9	-8.8	29.4	31.1
-12.2	-7.2	32.2	33.3
-9.4	-5.5	34.9	34.9
-6.6	-3.8	37.7	36.6
-3.8	-1.6	40.5	38.2
-1.1	0	43.3	40.5
1	1.6		
4.4	3.3		
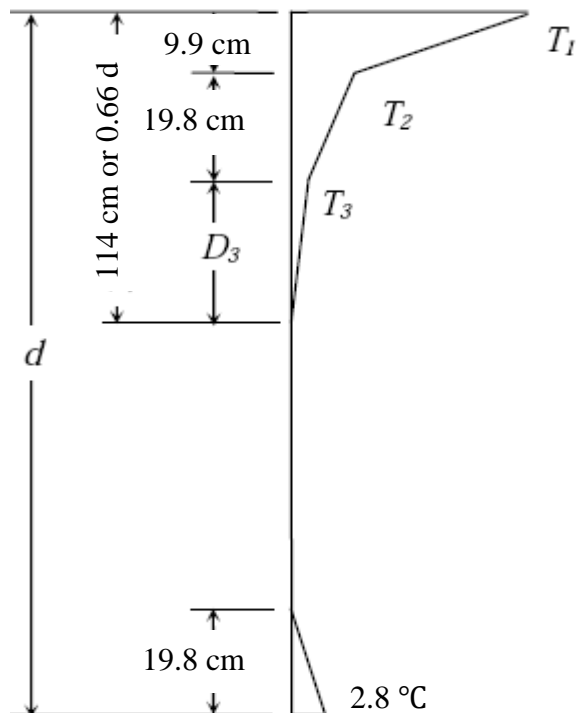
Figure 2.6 Vertical thermal gradients of concrete bridge superstructures [40]

Table 2.4 Values of the vertical thermal gradients [40]

Zone	T_1 (^{o}C)	T_2 (^{o}C)	T_3 (^{o}C)
1	12.2	-10	-15
2	7.7	-11.1	-15.5
3	4.9	-11.6	-15.5
4	3.3	-12.7	-16

2.7 AASHTO LRFD Bridge Design Specifications [41]

More detailed information on thermal loading is provided in the AASHTO LRFD Bridge Design Specification 2010 than the AASHTO Standard Specifications. The LRFD Specifications indicate that the design thermal movement associated with a uniform temperature change can be calculated using either Procedures A or B which are discussed in the following subsection:

2.7.1 Temperature range for procedure A

Procedure A is in the AASHTO LRFD Specification 2010 at section C3.12.2.1 a method that has been used for bridge design, a moderate climate may be determined by defining the number of freezing days per year. If the number of freezing days is less than 14, the climate is to be moderate. Freezing days are days when the average temperature is less than 0 ℃ Table 2.5 shows the range of temperature. The difference between the extended lower or upper boundary and the construction temperature assumed in the design shall be used to measure the thermal effects.

Table 2.5 Procedure A temperature ranges

Climate	Steel or Aluminum (℃)	Concrete (℃)	Wood (℃)
Moderate	0 to 66.6	5.5 to 44.4	5.5 to 41.6
Cold	-16. 6to 66.6	0 to 44.4	0 to 41.6

2.7.2 Temperature Range for Procedure B

The Procedure B design was used a design temperature range defined through a thermal contour map of the United States. The temperatures provided in the maps are extreme bridge design temperatures for an average history of 70 years with a minimum of 60 years of data for many locations in the United States.

The design values between contours should be calculated by linear interpolation the largest adjacent contour may be used the maximum design bridge temperature and the smallest adjacent contour may be used the minimum design bridge temperature .

The minimum and maximum design temperatures should be noted on the drawings for the girders, expansion joints and bearings. The temperature range defined as the difference between the maximum design temperature and the minimum design temperature.

For all concrete girder bridges with concrete decks the maximum design temperature shall be determined from the contours of Figure 2.7 and the minimum design temperature shall be determined from the contours of Figure 2.8.
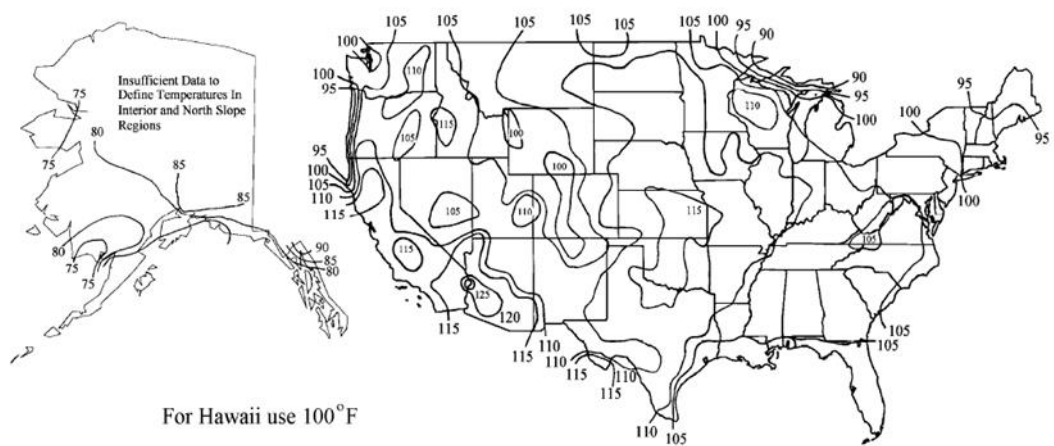
Figure 2.7 Contour maps of maximum temperature design for   concrete girder bridges with Concrete decks
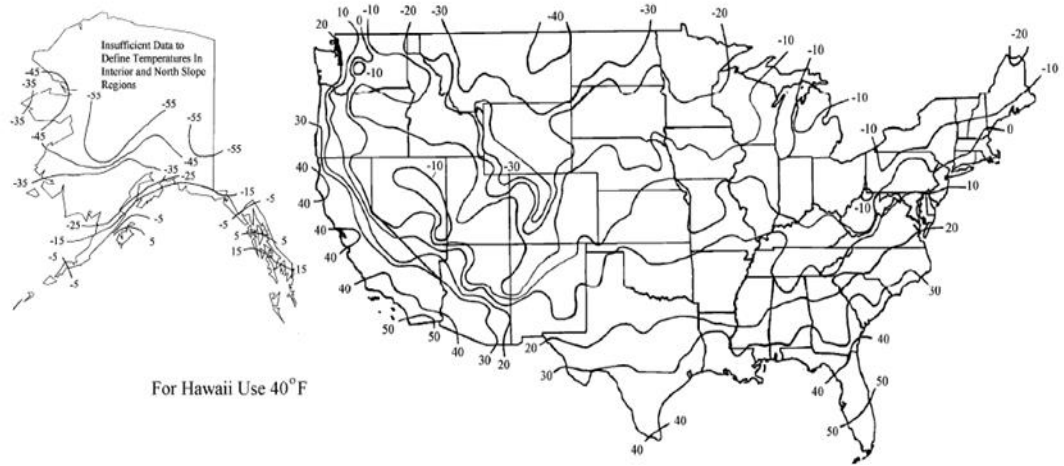
Figure 2.8 Contour maps of minimum temperature design for concrete girder bridges with concrete decks

The German code, DIN1072 [42] allowed to a thermal distribution which reduces linearly from the top surface to the soffit of a cross section of the bridge by 5°C, and the effective temperature average is 20 °C maximum and -30°C minimum. Figure 2.9 shows the proposed of the DIN1072 code.
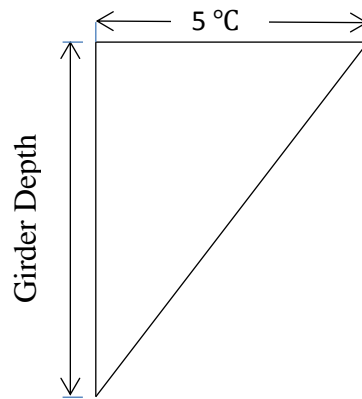
Figure 2.9 Temperature gradients suggested by the DIN1072 code [42].

CHAPTER 3

EXPERIMENTAL WORK

3.1 Introduction

The experimental work used in this study is a part of an experimental program carried out in the campus of Gaziantep University [43], in which the construction and instrumentation of a full-scale box-girder segment are utilized to study the thermal behavior of concrete bridge girders subjected to variable environmental thermal loads during the early age of concrete.

A full-scale concrete bridge box-girder segment was constructed and instrumented with thermocouples along and across the webs and the flanges to investigate the temperature distributions and gradients in concrete bridges during the early ages. During the early age of the concrete structure, the heat produced by the hydration of cement controls the concrete thermal behavior. If concrete is exposed to an open environment, it is exposed to continuous change of climate. Thus, the solar radiation and the fluctuated ambient air temperature have also their effective contribution in the heat transfer process that occurs within the body of the bridge girder.

3.2 The Bridge Box-Girder Segment

The site of the box-girder segment was chosen so that the shadows from the surrounding buildings have no significant effect on thermal loadings of the bridge segment. Figure 3.1 shows the details of the geometry of the tested box-girder segment, while Figure 3.2 shows the form working of the box-girder segment. As shown in Figure 3.2, the box-girder segment is constructed on a reinforced concrete frame.

The reinforced concrete frame was used to raise the experimental segment, so that the air can flow freely on the bottom surface of the segment and the solar radiation

and the ground reflected radiation could reach the bottom surface of the segment. Figure 3.3 shows the box-girder segment after formwork removal, which reveals the detail dimensions shown in Figure 3.1.

It should be mentioned here that the box-girder segment was constructed using two truck mixers, the first was used for the bottom flange, while the webs and the top flange was poured using the second truck mixer. The time lag between the two patches was about 50 minutes.
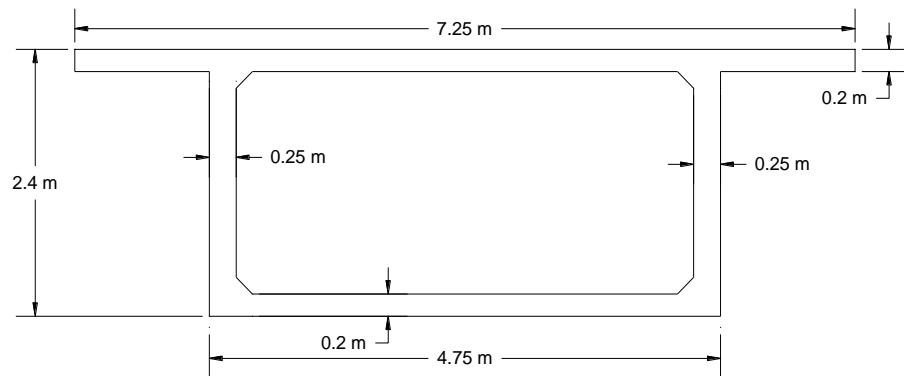
Figure 3.1 Dimensions of the cross-section of the bridge box-girder segment

Figure 3.2 The formwork of the experimental box-girder segment

Figure 3.3 The box girder segment and the after formwork removal

3.3 Instrumentation of the Box-Girder Segment

To measure the environmental thermal loads those have contributions in the heat transfer process occurs in the box-girder segment, the following sensors were installed in the field of the experimental work.

1. Air temperature probe, which contains a high accuracy thermistor, was used to measure the shade air temperature at the site. To eliminate the effect of solar radiation on the temperature accuracy, the probe was contained inside a solar shield.
2. Pyranometer, which was used to measure the global solar radiation intensity on horizontal surfaces.
3. A three-cup anemometer, which was used to measure the wind speed in the site of the experimental work.

3.3.1 Thermocouples

Thermocouples were installed in different locations inside the top flange, the bottom flange, and the two webs to monitor the concrete temperature along the different parts of the box girder segment.

Table 3.1 lists the number and the location coordinates of the used thermocouples considering the origin at the center of the lower face of the bottom flange. All the

installed thermocouples were Type-T, which has higher accuracy than the other known types of thermocouples. The maximum temperature error for the used thermocouples is ± 0.5 for temperatures between −40 °C and 125 °C.The thermocouples of the south web, the north web, the top flange, and the bottom flange were denoted by the letters SW, NW, TF, and BF then followed by the number of the thermocouple as shown in the Table 3.1.

Table 3.1 Numbering and coordinates of thermocouples.

TC No.	X (m)	Y (m)	TC No.	X (m)	Y (m)
SW1	-2.25	2.4	NW12	2.25	0.8
SW2	-2.25	2.36	NW13	2.25	0.4
SW3	-2.25	2.32	TF1	-3.625	2.3
SW4	-2.25	2.28	TF2	-3.125	2.3
SW5	-2.25	2.24	TF3	-2.625	2.3
SW6	-2.25	2.2	TF4	-1.5	2.3
SW7	-2.25	2	TF5	-0.75	2.3
SW8	-2.25	1.6	TF6	0	2.4
SW9	-2.375	1.2	TF7	0	2.3
SW10	-2.25	1.2	TF8	0	2.2
SW11	-2.125	1.2	TF9	0.75	2.3
SW12	-2.25	0.8	TF10	1.5	2.3
SW13	-2.25	0.4	TF11	2.625	2.3
NW1	2.25	2.4	TF12	3.125	2.3
NW2	2.25	2.36	TF13	3.625	2.3
NW3	2.25	2.32	BF1	-2.375	0.1
NW4	2.25	2.28	BF2	-1.5	0.1
NW5	2.25	2.24	BF3	-0.75	0.1
NW6	2.25	2.2	BF4	0	0.2
NW7	2.25	2	BF5	0	0.1
NW8	2.25	1.6	BF6	0	0
NW9	2.375	1.2	BF7	0.75	0.1
NW10	2.25	1.2	BF8	1.5	0.1
NW11	2.125	1.2	BF9	2.375	0.1

As shown in the Figure 3.4, a total number of 48 thermocouples were utilized to investigate the temperature distribution in the concrete box girder during the early ages. 26 thermocouples were installed in the webs, while 13 thermocouples and 9 thermocouples were installed in the top and the bottom flanges, respectively.

The thermocouples from SW1 to SW13 refers to the thermocouples instrumented in the south wall. NW1 to NW13 refer to the thermocouples of the north wall. TF refers to the thermocouples installed in the top flange. BF refers to the thermocouples of the bottom flange.

Note: all dimensions in meter
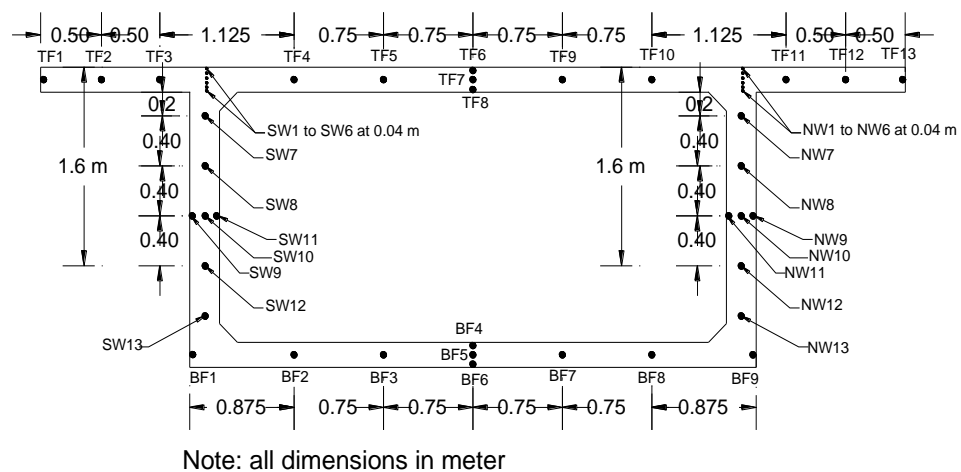
Figure 3.4 The location of thermocouples for the cross section of box girder segment

3.3.2 Data acquisition

The data logger is used to read and record the continuous readings from the air temperature probe, the pyranometer, the anemometer, and the 48 thermocouples. The data logger capacity is limited for less number of connected sensors; therefore, two multiplexers are connected to the data logger to increase the connection capacity of the data acquisition system. With each of which, 32 sensors can be simultaneously recorded. Figure 3.5 shows the data logger, while Figure 3.6 shows the box that contains the data logger and the multiplexers.
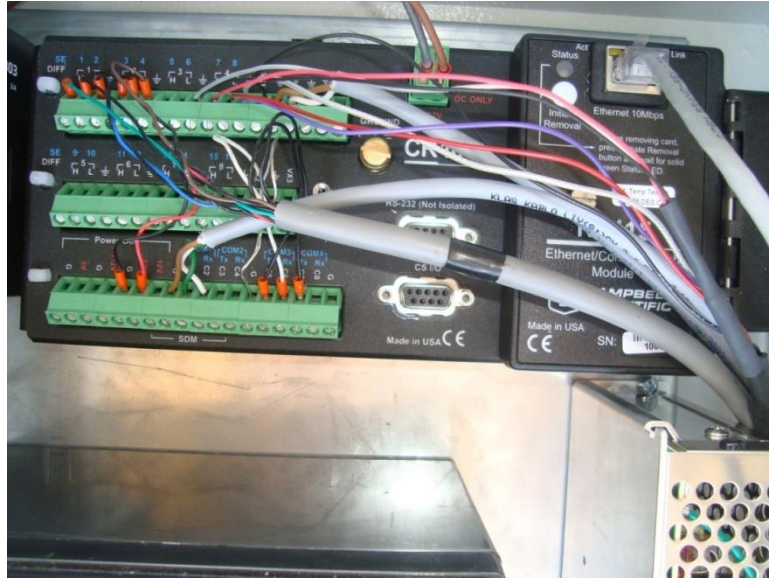
Figure 3.5 The data logger used in the study

Figure 3.6 The environmental containers that contains the data acquisition system
and the instrumented thermocouples

CHAPTER 4

RESULTS AND DISCUSSION

4.1 Environmental Thermal Loads

As mentioned in the previous chapter, three environmental sensors were installed in the experimental box-girder bridge segment to record the environmental thermal loads. Air temperature probe with solar shield was installed to monitor the temperature of the ambient air, pyranometer was installed to monitor the global solar radiation, while an anemometer was installed to monitor the speed of the wind.

Figure 4.1 shows the air temperature records for the first five days (120 hours) after the cast of the bridge segment (11:30 a.m. on May 25). It is clear from Figure 4.1 that air temperature during the five days fallen in the range of about 10℃ to about 30℃.
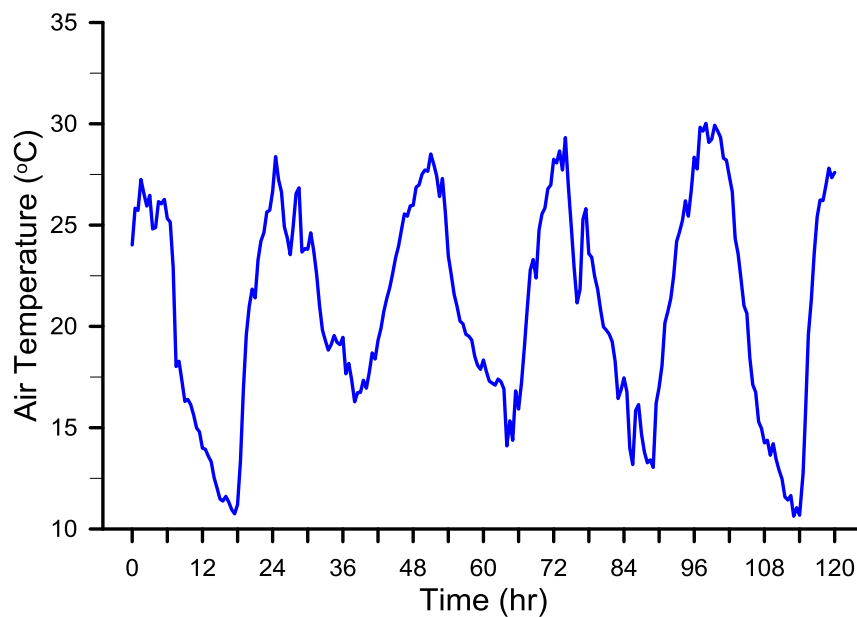
Figure 4.1 Air temperatures during the first 120 hours

Figure 4.2 shows the records of solar radiation during the same period. The fluctuation of solar radiation reflects the state of the cloud cover during these days. It is clear that the sky was partially cloudy during the first day, since the solar radiation records show high frequency fluctuation. The day after the concrete pouring was also partially cloudy, as shown in Figure 4.2, but with lower rates of fluctuation. Similar results are shown in the fourth and the fifth days. The sky was sunny during the full day hours of the third day as clearly illustrated in Figure 4.2. The maximum recoded hourly solar radiation during the five days was more than 1000 W/m^2, which was recorded during the fourth day.
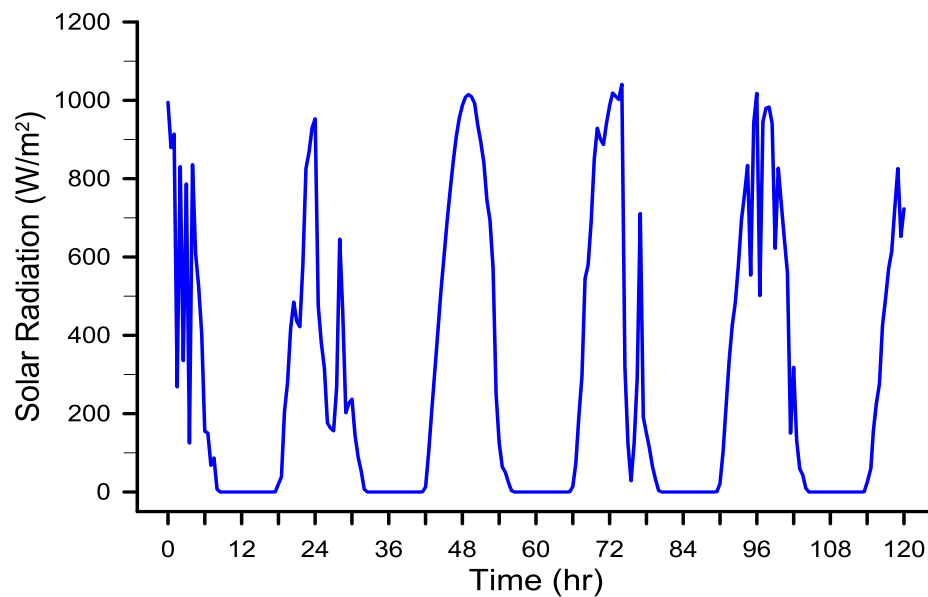
Figure 4.2 Solar radiation during the first 120 hours

Figure 4.3 shows the records of wind speed during the first five days after concrete pouring. It is clear that the wind speed was noticeably fluctuated during the full 120 hours. The wind speed during this period ranged from 0 m/s to about 3.0 m/s.
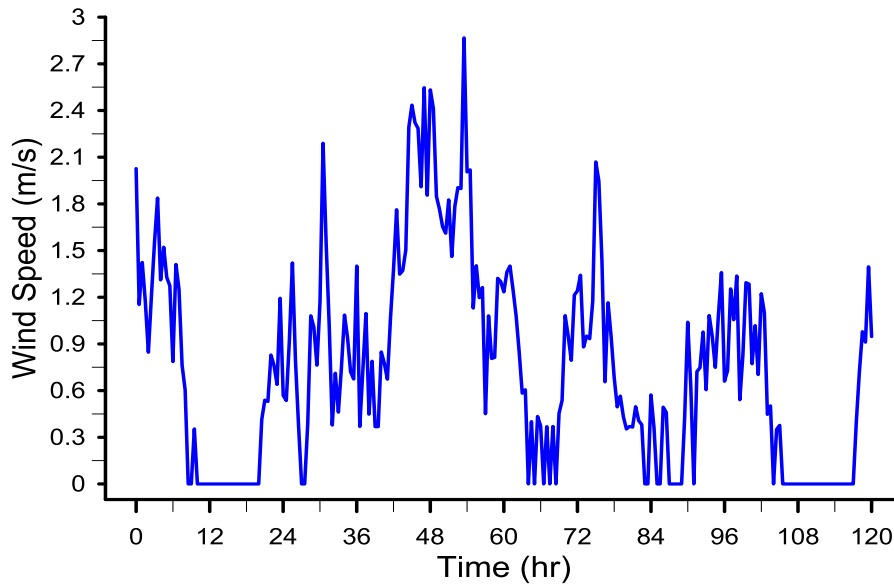
Figure 4.3 Wind speed during the first 120 hours

4.2 Temperatures-Time Behavior

The behavior of temperature with time is different from a thermocouple to another, but a general behavior can be distinguished for each one of thermocouples. The effect of hydration heat is also clear.

Figure 4.4 shows the temperature-time curves for the thermocouples that installed within the 0.2 m depth of the top flange. These thermocouples start at the top surface of the top flange with SW1 and end with SW6. Figure 4.5 shows the thermocouples SW7 to SW13 that installed along the web.

It is shown from the observation of Figure 4.4 that the effect of the heat of hydration dominates the temperature-time curve behavior during the first two days after the cast of concrete. The heat generated in concrete due to cement hydration clearly increases the temperature of concrete. The significant temperature increase starts after about 4 to 5 hours from concrete pouring, and continue to reach maximum temperature after about 10 to 12 hours from concrete pouring. After which, the concrete hydration heat tends to decrease significantly within the next 24 hours, showing lower temperature readings.

The effect of heat of hydration on the temperature-time curve relationships depends upon on the location of the thermocouples. The thermocouples that located near the surface display different behavior from the interior thermocouples. In addition,

32

different levels of influence can be observed between the interior thermocouples themselves. As a thermocouple embedded in a larger volume of concrete, the released heat of hydration increases and its effect becomes more dominator on the temperature-time curves. Oppositely, as the surrounding concrete volume decreases, the influence of the heat of hydration decreases.

As shown in Figure 4.5 the thermocouple SW7, which is located at the slab-web junction shows higher temperatures than all other thermocouples. As shown in Figure 3.4 and listed in Table 3.1, SW7 is the thermocouple surrounded by the largest concrete volume compared to other thermocouples. It is surrounded by 0.4 m of concrete from the top and the concrete of the 0.15 m × 0.15 m hunch at the interior cavity of the box-girder segment.

The thermocouples that located near the surface behave differently, with lower degree of temperature increase. As shown in Figure 4.4, the surface thermocouple SW1 shows the lowest temperature during the first 12 hours, in which heat of hydration effect is maximized. SW2, SW3, and SW4 show higher dependency on hydration heat compared to SW1, but still much lower than SW7.

 It is clear from Figure 4.4 of the temperature-time curves of the thermocouples SW1 to SW6 (within the top slab) that as the concrete cover increases (distance from the top surface of the top slab), temperature increases. The temperature of SW6 is higher than the temperature of SW5, which is higher than SW4 and so on.
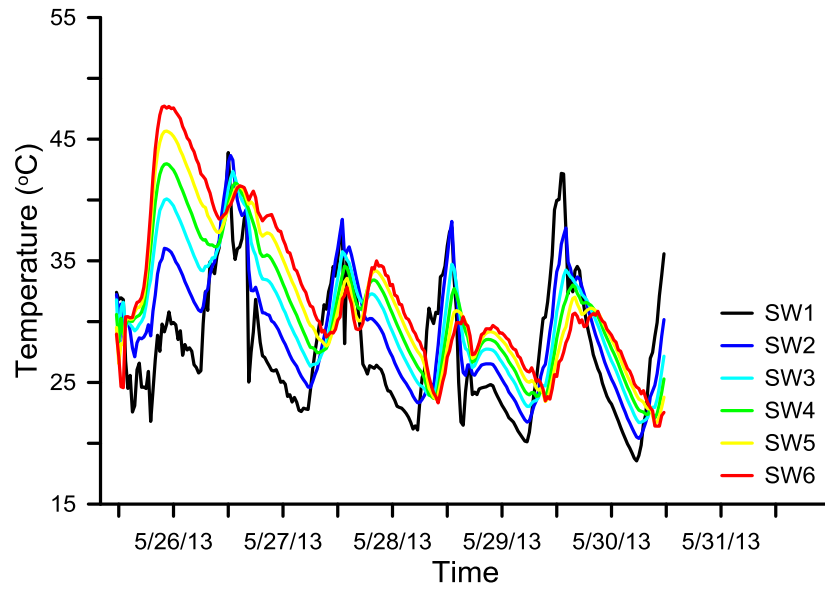
Figure 4.4 Temperature-time curves the thickness of the top flange (SW1to SW6)
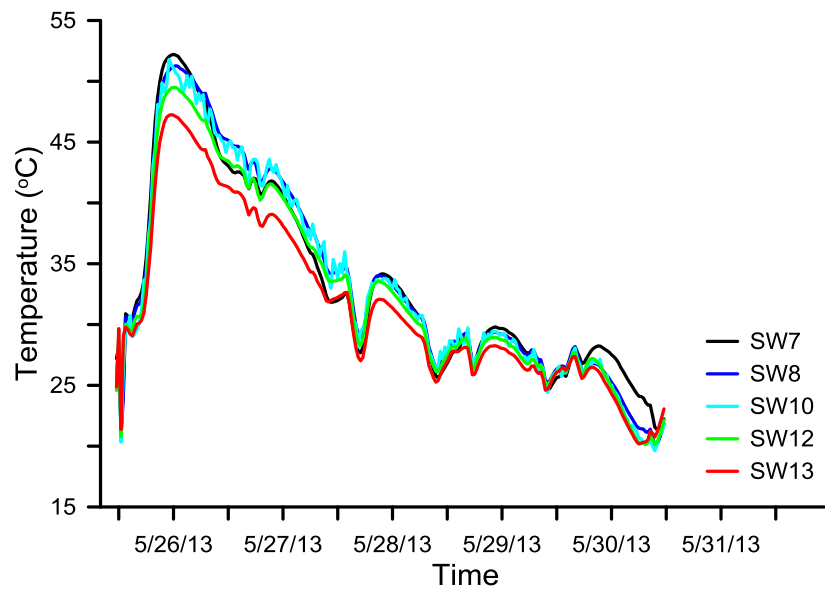
Figure 4.5 Temperature-time curves for the South Web group

Figure 4.6 shows the temperature-time curves of the north web's thermocouples. These thermocouples start at the top surface of the top flange with NW1 to NW6. Figure 4.7 shows the thermocouples NW7 to NW13 that installed along the north web.

The north web thermocouples display exactly the same behaviors as those of the south web's thermocouples. NW7 and NW8 show the higher the effect of heat of hydration with the higher altitude of the temperature-time curves compared to other

thermocouples. NW7 is installed in a similar location as for SW7, thus it is surrounded by the large volume of concrete. This explains why NW7 and NW8 have the highest temperatures among all thermocouples. NW1 to NW6 are the thermocouples embedded along the thickness of the top slab. These thermocouples show similar behavior as thermocouples SW1 to SW6. NW1 show the lowest temperature, while NW2 shows a little higher temperature and so on.
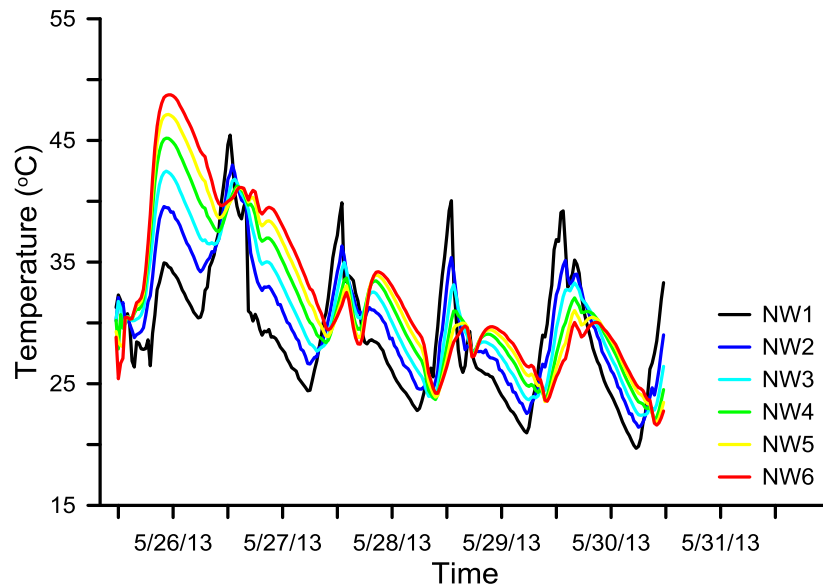
Figure 4.6 Temperature-time curves the thickness of the top flange (NW1to NW6)

Figure 4.7 Temperature-time curves for the North Web group

Figures 4.8 and 4.9 display a comparison between the temperature-time curves of some selected thermocouples, which are installed along the south web of the box girder in addition to the air temperature-time curve. The thermocouples were selected from different locations along the south web to represent the temperature distribution of concrete. SW1 is the top surface thermocouple.
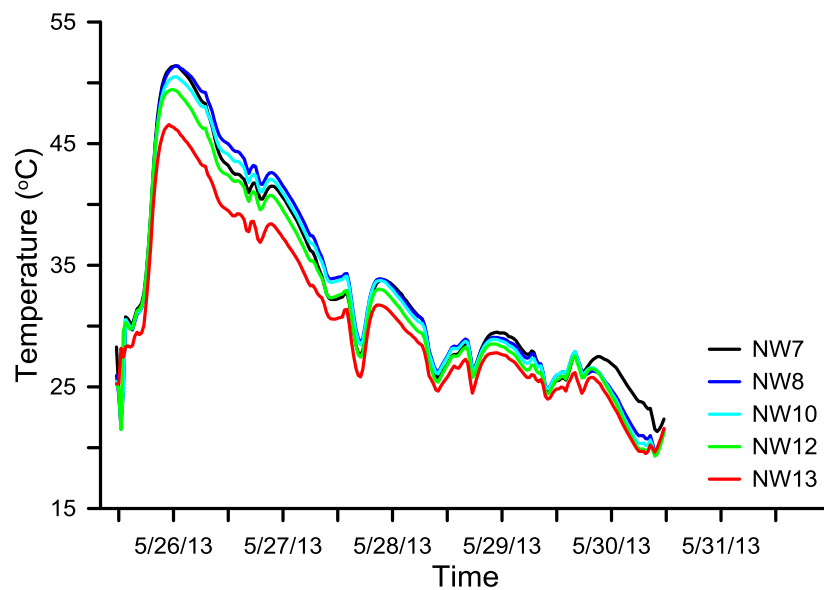
SW7, is the thermocouple located 0.4 m from the top surface and is surrounded by the largest concrete volume, while SW4 (0.12 m from the top surface) is located between SW1 and SW7. Moreover, SW12 is located at 1.6 m from the top surface of the top slab. All the selected thermocouples are embedded along the centerline of the thickness of the web of the box girder segment.

As shown in Figure 4.8, SW1, which is the surface thermocouple, seems to follow the same temperature-time behavior of air temperature. This is an expected result, since it is almost exposed directly from the top to air and it is surrounded with the smallest volume of concrete. The temperature of SW1 increased during the daytime hours, reaching its maximum after the midday, and decreased during the late day hours and night hours, reaching its minimum before sunrise. SW1 followed the air temperature behavior and it was almost not affected by the heat of hydration of the concrete box girder.

SW7 in Figure 4.9 showed no dependency on air temperature during the first 48 hours, in which the effect of heat of hydration was maximized. During this period, the temperature-time curve of SW7, was completely controlled by the heat of hydration behavior. Where the temperature of SW7 stilled continues to increase during the night hours of the first day. Thus, it was not affected by the cooling air (convection) during the night hours.

The temperature-time curves of SW4 and SW12 showed a mixed behavior, in which dependency is shown on both hydration heat and air temperature as shown in Figure 4.9 the temperature increased during the first hours of the night of the first day because of the heat of hydration, while after midnight SW4, which is located at 0.12 m from the top surface of the top slab showed some temperature decrease due to the with the same concrete covers, but the location of SW4 near the top surface of the top slab, in which the convection is maximum forced SW4 to show the highest

degree of dependency on air temperature than SW12 convection cooling of air, while SW12 tended to be close to the behavior of SW7.

This mixed behavior can be attributed to the quantity of concrete covering the thermocouple and the location of the thermocouple. SW4 and SW12 almost cover. The maximum recorded temperature at SW7 is 52.2 ℃, which was recorded at midnight of the first day, while air temperature at the same time was 14 ℃ only. Table 4.1 shows the temperature distribution along the south web during the first 12 hours (at the midnight) after the concrete pouring.

Table 4.1 The temperature distribution along the south web

Dates	No. thermocouple	Temperature (℃)
26 May 12:00 a.m. (After 12.5 hours of concrete casting)	SW1	30
	SW4	42.46
	SW7	52.21
	SW12	48.14

As shown in Figures 4.8, and 4.9 the temperature of SW1 (at the top surface) increased with the increase of air temperature, reaching 43.9 ℃ in the mid of the next day, while the temperature of the interior thermocouples SW4, SW7 and SW12 showed continuous decrease without being affected by the increased air temperature.

After 48 hours, the effect of heat of hydration decreased and the temperature-time curve of SW7 showed some dependency on the fluctuation of the air temperature with time, in which the temperature increases during day hours and decreases during night hours.
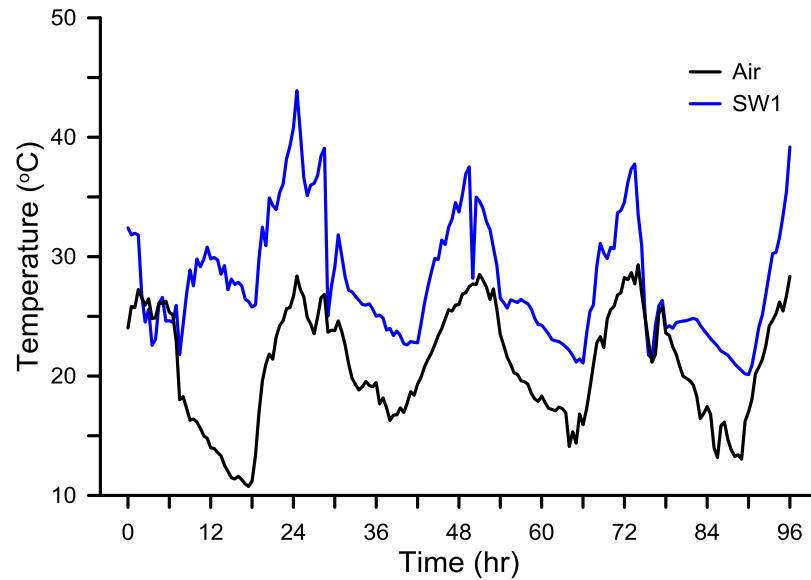
Figure 4.8 Temperature-time curves for SW1 with air temperature
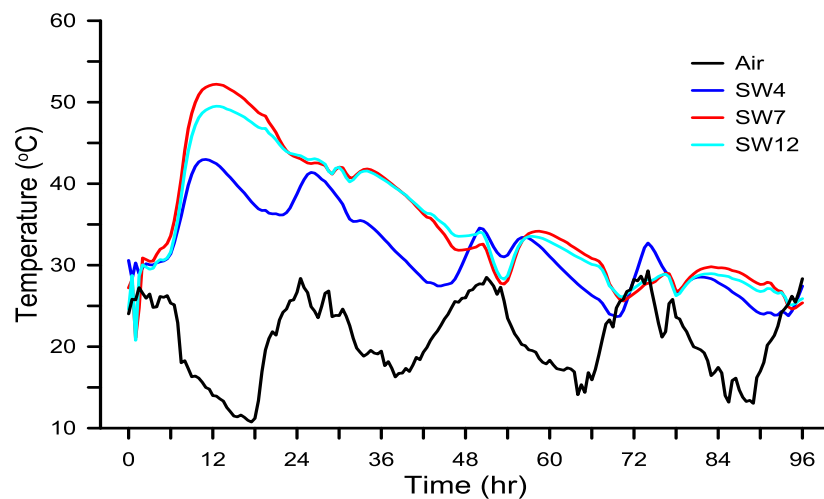
Figure 4.9 Temperature-time curves for SW4, SW7 and SW12with air temperature

Figure 4.10 and 4.11 show the temperature-time curves of selected thermocouples along the north web versus the air temperature-time curve. The selected thermocouples are NW1, NW4, NW7, and NW12. These thermocouples have the same locations as for south web, but installed along the centerline of the north web. The behavior of the different thermocouples was similar to those of the south web. At Figures 4.10 and 4.11 thermocouple NW1 at the top surface of the box girder followed the air temperature behavior, while interior thermocouples showed higher dependency on the heat of hydration rather than on the air temperature. The degree of this dependency depends on the location of the thermocouple and the amount of concrete surrounding it. Table 4.2 shows the temperature distribution of north web.

Table 4.2 The temperature distribution along the north web

Dates	No. thermocouple	Temperature (℃)
26 May 12:00 a.m. (After 12.5 hours of concrete casting)	NW1	34.12
	NW4	44.84
	NW7	51.36
	NW12	49.44
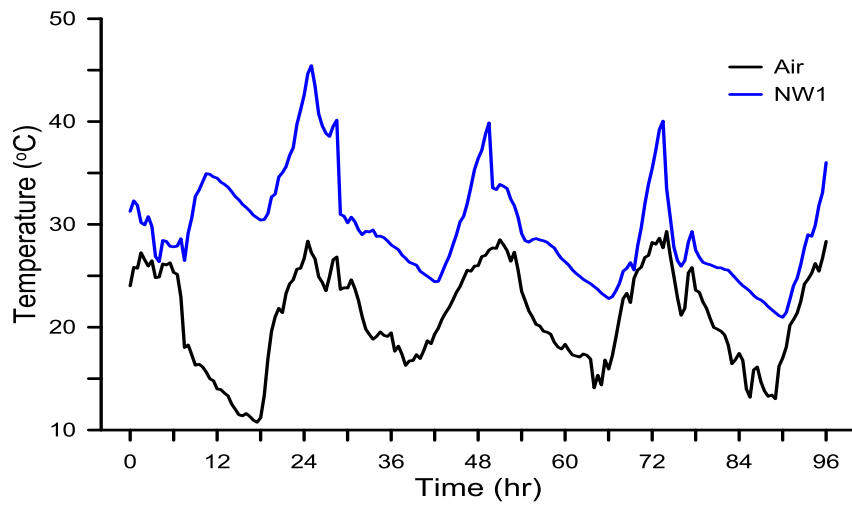
Figure 4.10 Temperature-time curves for NW1 with air temperature

Figure 4.11 Temperature-time curves for NW1, NW4, NW7 and NW12 with air temperature
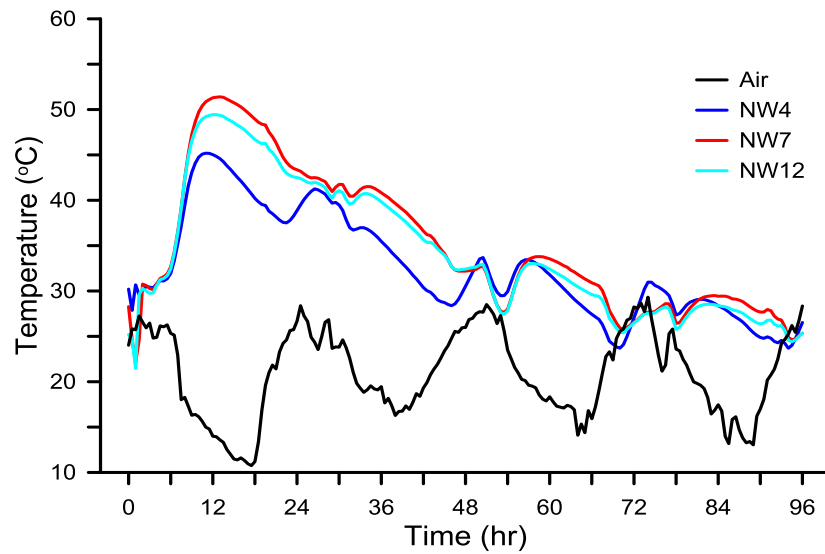
4.3 Vertical Temperature Distribution

The vertical temperature distribution along the depth of bridge superstructures is important to monitor the stresses that may appear from the temperature differences in the superstructure. Figure 4.12 shows the locations of thermocouples along the south and north webs of the concrete box girder segment.
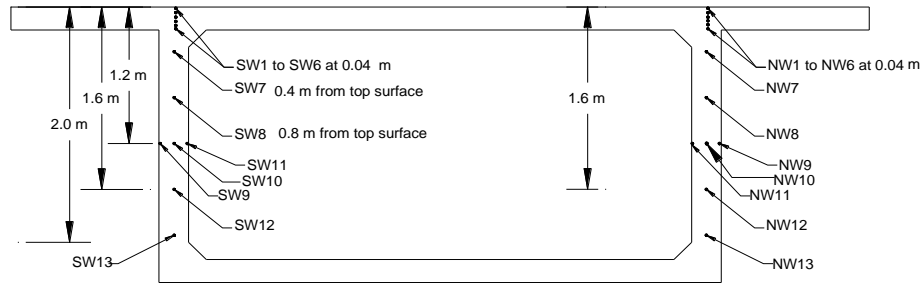
Figure 4.12 The locations of thermocouples along the cross section of the south and north webs

It is well known that almost during the whole daylight hours, the top surface is directly exposed to solar radiation and for this reason, it absorbs higher thermal radiation from the sun than the other parts of the box girder bridge. The absorption of the higher percentage of solar thermal radiation leads to heat gain, therefore increases the temperature of the top surface. During the hot day hours after the midday, the top surface reaches its maximum temperature, however at the same time the cores of concrete are still cold, which leads to high temperature difference along the depth of the box girder, which is also described as the temperature gradient.

Oppositely, and during night hours, the quick cooling of the top surface leads to a quick reduction in the temperature of the surface. The concrete cores lose heat slowly because of the low thermal conductivity of concrete, which leads to a negative thermal gradient, with the minimum temperature at the top surface and the maximum at the concrete cores.

Figure 4.13 shows the temperature distribution along the depth of the south web during the first day only (May 25) until the midnight, which are the temperature distributions at 1:30 p.m. (about 2 hours after the concrete pouring), 3:00 p.m. (after

about 3.5 hours), 6:00 p.m. (after about 6.5 hours), 9:00 p.m. (after about 9.5 hours) and 12:00 a.m. (after about 12.5 hours).

From the observation of Figure 4.13, it is shown that the temperature is almost uniform along the depth of the south web at 1:30 p.m. and 3:00 p.m. on the first day. This is because the initial temperature of concrete controls at this time and only a limited amount of heat was generated in this period.
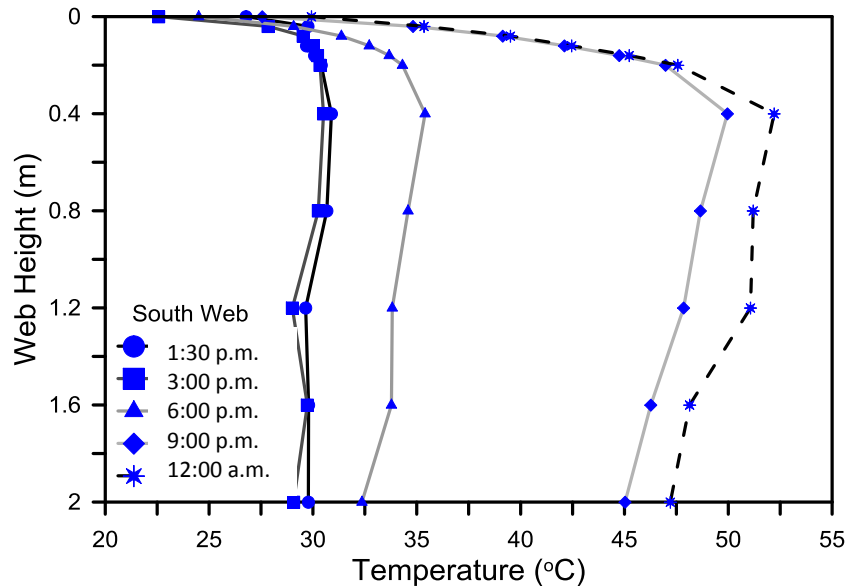
Figure 4.13 Vertical temperature distributions along the SW for selected time steps during the first day after concrete casting

This observation is clear in Figure 4.14 for the north web. The temperature during the 1:30 p.m. and 3:00 p.m. was almost constant along the web, which were approximately 30 ℃. At 6:00 p.m. on the first day, the concrete temperature increased due to the released heat of hydration, which affected the concrete temperature. The highest temperatures recorded at this time were about 35.4 ℃ and about 34.25 ℃ at thermocouples SW7 and NW7 in the south and the north webs (both located 0.4 m below the top surface).

At 9:00 p.m. and 12:00 a.m. (midnight of the first day) and as shown in Figures 4.13 and 4.14, it is clear that the hydration heat had a noticeable effect on the concrete temperature of the south and the north webs of the box girder, where the concrete temperature along the clear height of the webs increased to temperature averages of about 46 ℃ and 50 ℃ at 9:00 p.m. and 12:00 a.m.

Figures 4.13 and 4.14 also confirm the discussion of the last section where the temperature was maximized (52.21 ℃ and 51.36 ℃) at the thermocouples SW7 and NW7, which are surrounded by the largest concrete mass. On the other hand, the air cooling affected the temperature of the top surface and the thermocouples that installed within the top slab thickness as shown in Figures 4.8 and 4.10. The temperature at the top surface was minimum at this time because of the convection cooling, which was about 31 ℃ and 34 ℃ in the south and the north webs.
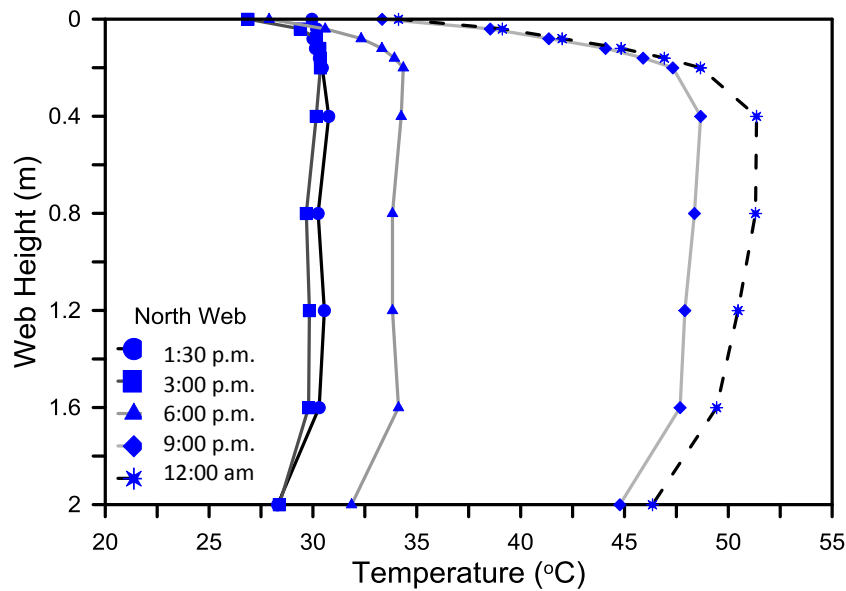
Figure 4.14   Vertical temperature distributions along the NW for selected time steps during the first day after concrete casting

During day hours, the temperature of the top surface of the hardened concrete should be higher than that of other interior parts, but in the current study, the temperature at the top surface during the day hours of the next was lower than the interiors of the webs. This result is due to the magnitude of hydration heat that liberated during the first 24 hours from the casting of concrete. The heat of hydration increased the temperature of the interior parts of concrete, therefore it stilled higher than the temperature of top surface (top surface gained the temperature from solar radiation) until disappearance the effect heat of hydration.

The vertical temperature distributions were studied for five days from the cast of concrete to understand the limits of the effect of hydration heat on the vertical temperature distribution and to recognize the period of this effect.

Figures 4.15 and 4.16 show that the temperature distribution was almost constant at the 3:00 p.m. on the first day (May 25). This is because the initial temperature controlled at this time and the hydration process was in its initial stage.

The effect of heat of hydration was obvious after 24 hours and the webs temperatures of the box girder increased and reached higher than the temperatures of other days. As discussed in Figures 4.13 and 4.14, and which is also clear in Figures 4.15 and 4.16, the temperature increase of the top surface due to solar radiation was still less than the temperature caused by the heat of hydration in the second day. At the same time, the temperatures of the concrete cores were still higher than the temperature at the top surface.

After 48 hours, the influence of heat of hydration was significantly decreased, which is very clear in the temperature distribution curves of the last three days. As shown in Figures 4.15 and 4.16, the vertical temperature distributions in 27 , 28, and 29 May seem to follow the normal vertical temperature distribution of aged concrete, in which the temperature is maximum at the top surface due to the effect of solar radiation and the high air temperature around 3:00 p.m.
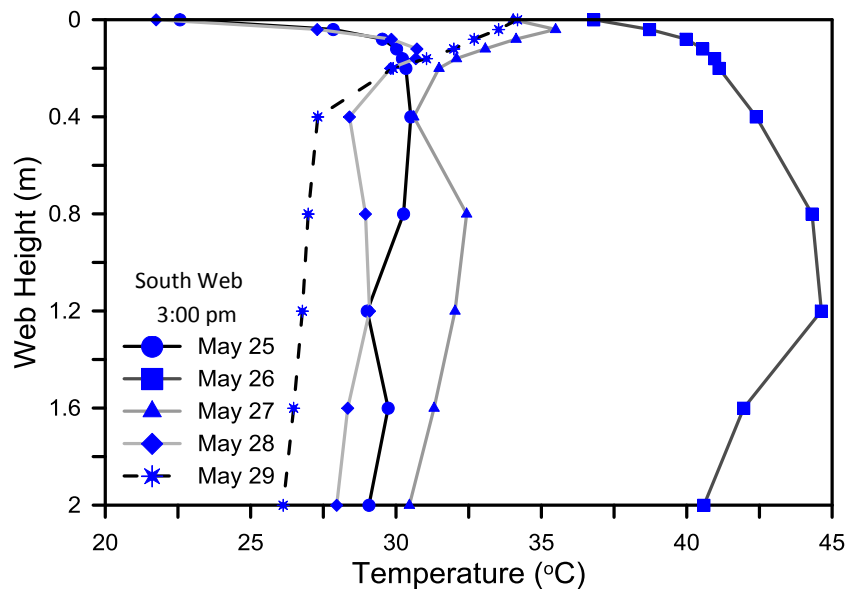
Figure 4.15 Vertical temperature distributions at 3:00 p.m. for five days (SW)

Another important notice is that the average temperature has also decreased with time after the first day. The ambient air temperature at 3:00 p.m. of the first four days was about 28 ℃, while for the fifth day it was about 30 ℃. Table 4.3 shows the maximum and the minimum temperature distribution along the south web of the box

girder segment. A similar sequence of results can be shown in Figure 4.16 for the north web. This means that the effect heat of hydration was almost diminished after about 100 hours. Table 4.4 shows that the maximum and the minimum temperature distribution along the north web of the concrete box girder segment
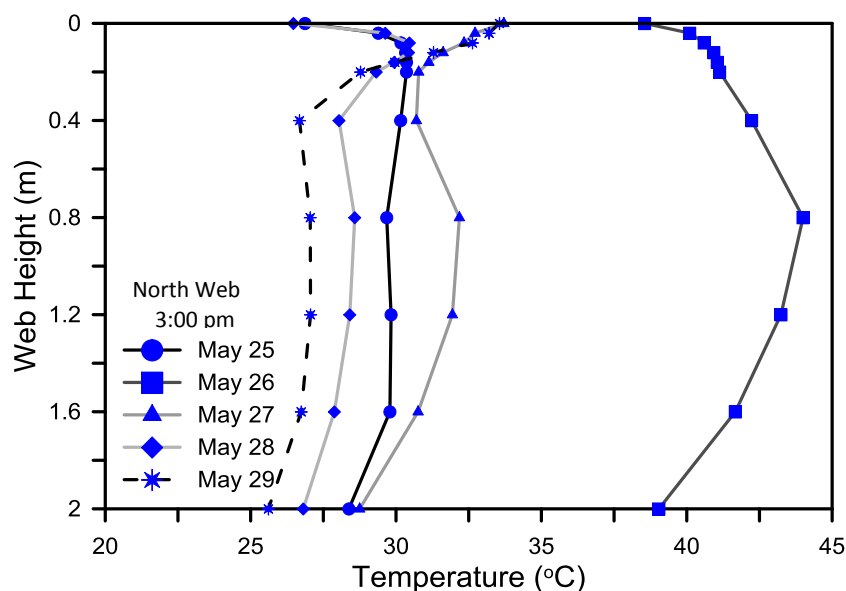
Figure 4.16 Vertical temperature distributions at 3:00 p.m. five days (NW)

Table 4.3 Maximum and minimum temperature distribution of SW during five days

No. thermocouple	Dates	Temperature (℃)	Air temperature (℃)
SW7	May 26 12:00 a.m	52.21 (maximum)	14
SW1	May 30 5:30 a.m.	18.55 (minimum)	10.68

Table 4.4 Maximum and minimum temperature distribution of NW during five days

No. thermocouple	Dates	Temperature (℃)	Air temperature (℃)
NW7	May 26 12:00 a.m	51.36 (maximum)	14
NW1	May 30 5:30 a.m.	19.69(minimum)	10.68

4.4 Lateral Temperature Distributions Along the Top Flange

At the top surface, eleven thermocouples were installed along the mid thickness of the top flange to study the lateral temperature distribution along the top flange. These thermocouples start with the southern vertical face of the top flange and ends with the northern vertical face of the top flange. The spacing between the thermocouples

along the southern and northern cantilever ends was 0.5 m, followed by one spacing of 1.125 m, then the typical spacing becomes 0.75 m tell the center of the top slab. In addition to the eleven thermocouples, one exterior thermocouple was installed on the top face of the top flange and other interior thermocouple was installed at the bottom face of the interior cavity. Figure 4.17 shows the locations of thermocouples of the top, bottom, and the thermocouples of the exterior and interior of the top flange of the concrete box girder segment.
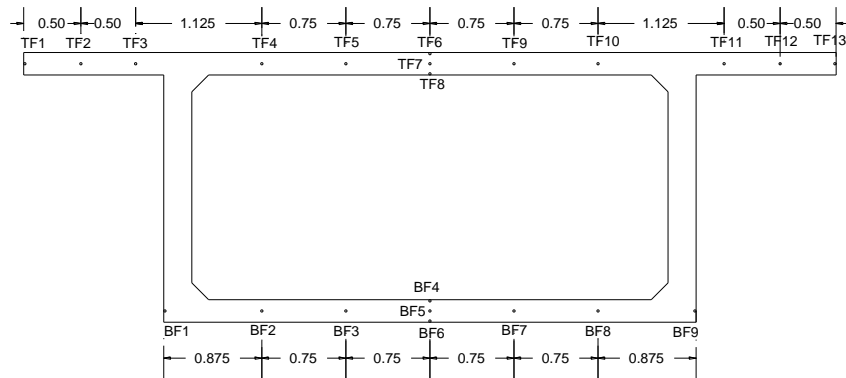
Figure 4.17 The location of thermocouples along the cross section of the top and bottom flange

Figure 4.18 shows the distribution of temperature along the width of the top flange .At 12:00 p.m. during the first day until the May 29. The selected time was 1:30 p.m. instead of 12:00 p.m. on the first day (May 25), because the cast of concrete of the top flange has not been finished yet at 12:00 p.m. As illustrated in Figure 4.18, the recorded temperatures were almost the same along the width of the top flange at 1:30 p.m. on 25 May, because the concrete has just been poured, and hence its initial temperature controls and this was an expected result.

It is also clearly illustrated in Figure 4.18 that the temperature of the top slab has increased significantly after 24 hours, which is also an expected result, this increase is attributed to the general increase in concrete temperature due to the heat of hydration. It is also shown in the figure that the thermocouple TF3 that is located near the top flange-south web hunch has recorded the maximum temperature of 37 ℃ (at 12:00 p.m. on 26 May). This is because the thermocouples at the flange-web hunch is the one surrounded by the biggest concrete mass among all of the top slab's thermocouples, hence the effect of heat of hydration was higher than the other parts.

Another important notice is that the thermocouple TF11, which is located near the top flange-north web hunch, has recorded a maximum temperature of 34.7 ℃ at 12:00 p.m. of the second day (26 May), which is less than that of TF3. This is because of the orientation of the longitudinal axis of the box girder bridge (East-West) and the season (end of spring), which caused that the south web subjected to higher heating than the north web during the day hours.

By the observation of Figure 4.18, it can be concluded that the temperature distribution along the top flange was uniform after 48 hours. This is generally because the effect of heat of hydration has decreased significantly after this period and it was almost negligible after 100 hours, which is obviously shown in the curves of the temperature distribution in 27, 28, and 29 of May shown in Figure 4.18.
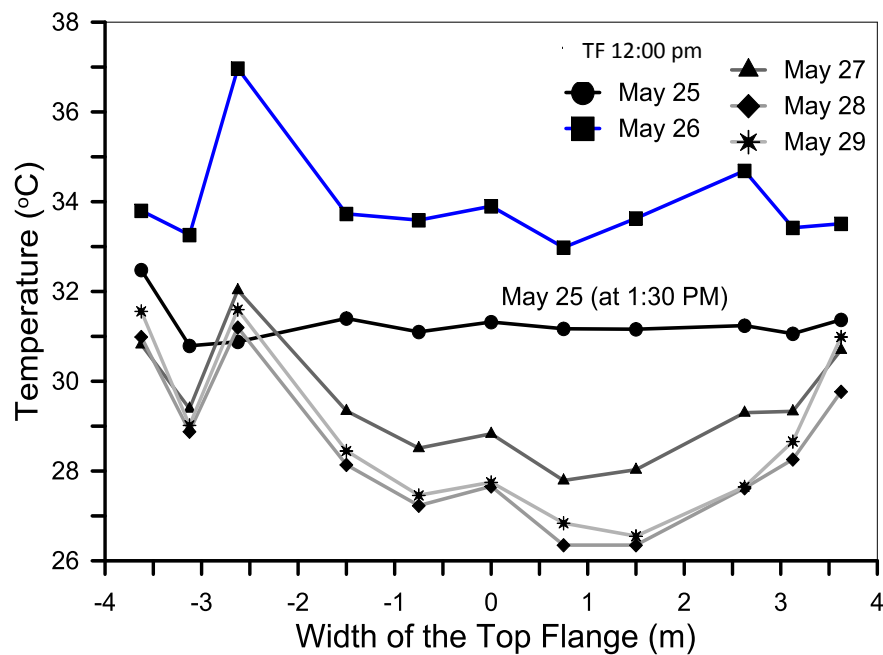
Figure 4.18 Temperature distributions along TF at 12:00 p.m. on the first five days

Figure 4.19 shows the temperature distribution almost uniform at the 25 May because the concrete at the initial temperature at this time expect the thermocouple TF13 was affected by solar radiation at the vertical face of the north web.

At the same figure shows that the behavior temperature distribution of the 26 May was affected by the hydration heat and recorded temperature higher than the others during the first 24 hours from the concrete pouring. Thermocouple TF3 recorded higher than the other thermocouples of the 27 and 28 May because, TF3 was located near the hunch of the cavity of box girder, and it kept the residual temperature of the

previous day due to the low thermal conductivity of concrete. At 29 May the temperature distribution was recorded higher than the 27 and 28 May because, at 3:00 p.m. of 29 May air temperature was recorded about 30℃. The maximum temperature at 29 May was 35.72 ℃, while the maximum temperature at 27 and 28 May were about 33 ℃ and 32 ℃ at the same time.
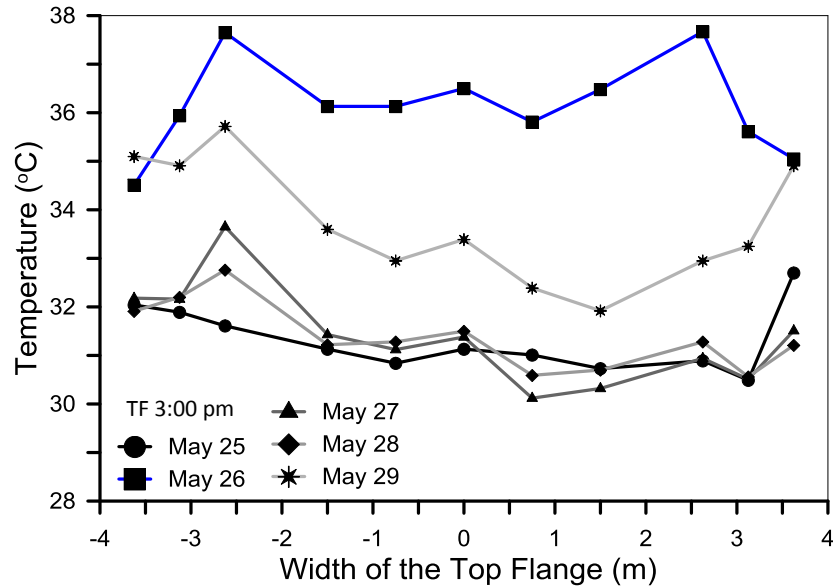
Figure 4.19 Temperature distributions along top flange at 3:00 pm on the first five days

Figure 4.20 also clears the effect of the heat of hydration, especially in the temperature distribution of the 25 May. On May 26 thermocouple TF11 was recorded temperature more than the other thermocouples because it kept the residual temperature of the previous period (3:00 p.m.) and affected by the solar radiation at the north web at this time compared with south web, where the orientation longitudinal axis (East – West) of the box girder. At 6:00 p.m. the temperature gradually diminished due to the sunset and disappearance the effect of solar radiation, therefore thermocouples at the outer end of the top flange (surface thermocouple) followed the fluctuation of the air temperature, while the rest thermocouples affected by slower ambient air temperature because of its location within the thickness of the top flange. At 28 May the temperature distribution was lower than the other days because the air temperature was low in the last 6 hours before the recording of temperature that day (about 22 ℃), while on 29 May the temperature recorded more than the 27 and 28 May due to the air temperature was about 26.65 ℃ at this time..

47
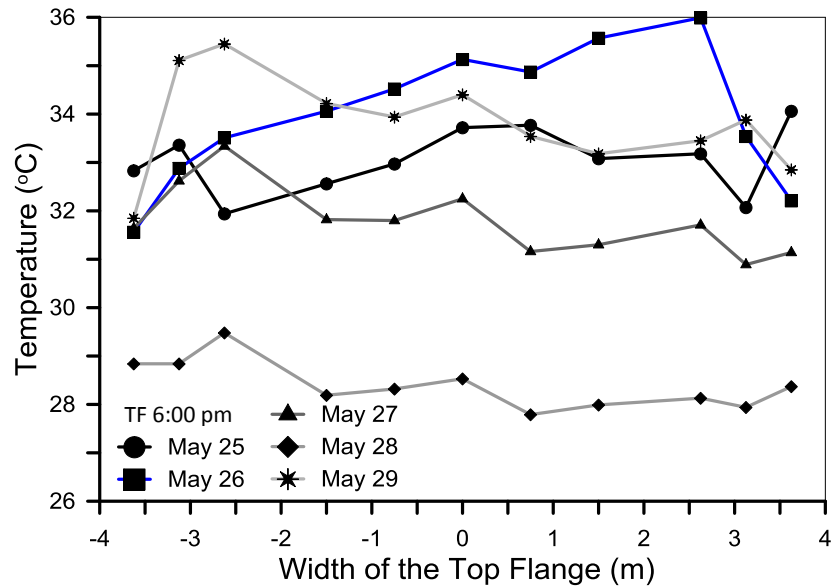
Figure 4.20 Temperature distributions along TF at 6:00 p.m. on the first five days

Figure 4.21 illustrates the temperature distribution along the top flange at 3:00 a.m. (early morning) during the first five days. On May 26, the maximum temperature was about 37 ℃ and it was higher than the maximum temperatures of the days 27, 28, 29 and 30 May. This means clearly that the effect heat of hydration was still maximum during the first night. In general, the temperature during the following four nights were lower than the temperature of the first night because the effect hydration heat has decreased with time.

As shown in Figure 4.21 and Table 3.1, the thermocouples TF1 and TF13 have recorded the minimum temperatures during the early morning of all days. This is simply because these thermocouples were located at the outer ends of the top flange and hence were directly subjected to the convection cooling of ambient air in addition to the effect of the surface cooling by long wave radiation to the surrounding atmosphere.

The air temperatures at 3:00 a.m. were 11.8, 16.7, 14, 12.5 and 11.0 ℃ on 26, 27, 28, 29 and 30 May, respectively. At the same time, the maximum temperatures of concrete at the top slab of box girder were 37.05, 28.38, 27.26, 25.53 and 25.88 ℃, respectively. This means the temperature of concrete with the time was approaching to the behavior of air temperature, and the influence heat of hydration was decreasing. Table 4.5 shows the maximum and the minimum temperature distribution along the top flange of the concrete box girder.

48
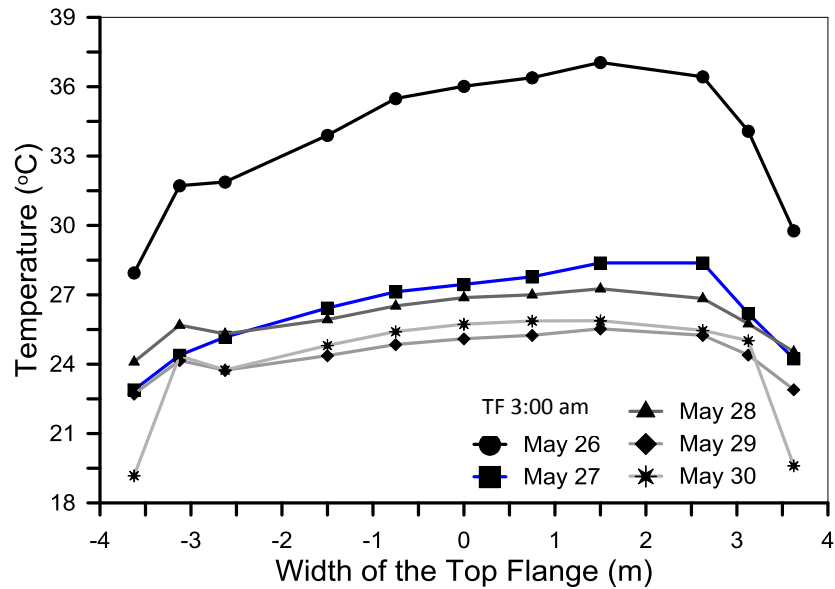
Figure 4.21 Temperature distributions along TF at 3:00 a.m. on the first five days

Table 4.5 Maximum and minimum temperature distribution of top flange

No.thermocouple	Dates	Temperature (℃)	Air temperature (℃)
TF10	May 25 9:30 p.m.	43.21 (max.)	16.14
TF1	May 30 5:30 a.m.	16.61 (min.)	10.68

4.5 Lateral Temperature Distributions Along the Bottom Flange

As shown in the Figure 4.17, seven thermocouples were installed along the mid thickness of the bottom flange to study the lateral temperature distribution along the bottom flange. These thermocouples start with the exterior southern face and ends near the northern face. One thermocouple was installed on the top face of the bottom flange and another was installed on the bottom face, while the other thermocouples was located at the mid thickness of the bottom slab.

Figure 4.22 illustrates the temperature distribution along the bottom slab of the box girder at 12:00 p.m. during the first five days. The selected time was 12:30 p.m. instead of the 12:00 p.m. on the first day (May 25) because the cast of concrete of the bottom flange has not been finished yet at 12:00 p.m.
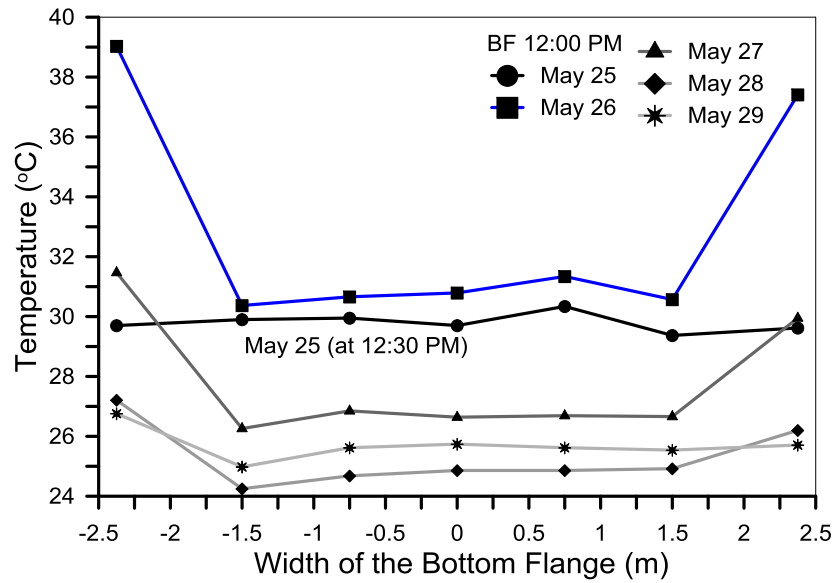
On May 25,   the temperature distribution was almost the same along the bottom flange at 12:30 p.m., because the concrete has just been poured at this time and its initial temperature controlled.

On May 26 (12:00 p.m, 24.5 hours after concrete casting), the temperature distribution along the bottom slab was almost the same except the thermocouples BF1 and BF9, which are located on the outer ends of the flange. The temperatures of BF1 and BF9 were about 39 and 37.4 ℃, which were more than the temperatures of the others thermocouples as illustrated in Figure 4.22. The temperatures of the interior thermocouples were controlled mostly by the hydration heat, while the concentration of solar radiation during the sunny hours before the noon of the day has increased the temperature of the surface thermocouples BF1 and BF9.

After 48 hours from concrete casting, the effect of heat of hydration was decreased and the temperatures in the following days (27, 28, and 29 May) were gradually depending on the ambient air temperature.

On 27 May (12:00 p.m., after 48.5 hours of concrete pouring), the effect of hydration heat on the average temperature of the flange has decreased significantly as shown in Figure 4.22. The temperature was almost stable along the interior length of the bottom flange, while the end thermocouples (BF1 and BF9) have recorded higher temperatures due to the effect of solar radiation and hot air. The recorded temperatures at BF1 and BF9 were 31.47 ℃ and 29.95 ℃, while the air temperature was about 27 ℃ at the same time.

The temperature distributions along the centerline of the bottom flange on 28 and 29 May were similar to that of 27 May. The temperature was nearly constant along the interior width of the flange, while temperature jumps occurred on the outer vertical surface of the flange. The maximum temperatures on 28 and 29 May were 27.2 and 26.8 ℃, while the air temperature at the same time was about 28.5 and 28 ℃, respectively.

Figure 4.22 Temperature distributions along BF for five days at 12:00 p.m.

Figure 4.23 shows the temperature distribution along the bottom flange at 3:00 p.m. during the five days. Excluding the temperature distribution of the first day, in general, the behavior of temperature at this figure was similar to the temperature distribution of Figure 4.22. At 3:00 p.m. and after many hours of surface heating due to solar radiation and hot air, the temperature of thermocouples BF1 and BF9 increase to greater than the temperature of the interior thermocouples.
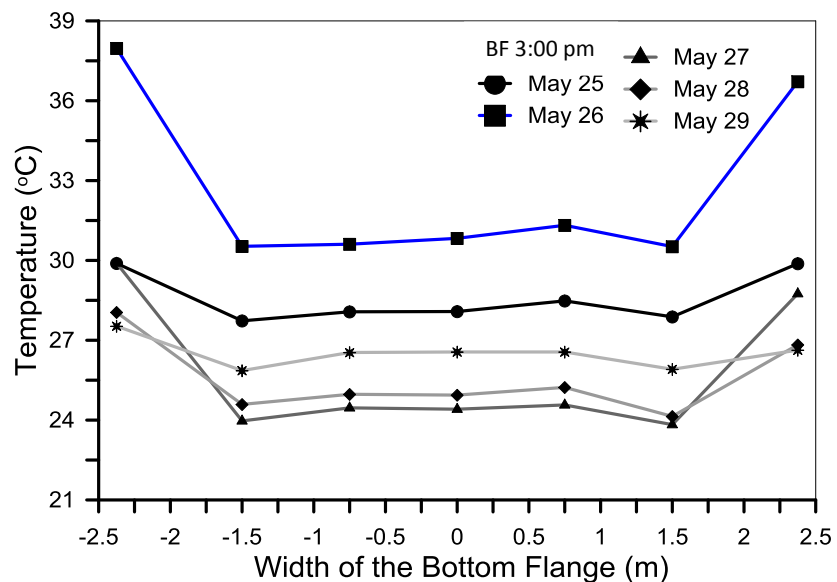
Figure 4.23 Temperature distributions along the bottom flange at 3:00 p.m.

Figure 4.24 shows the temperature distribution along the bottom flange at 6:00 p.m. during the first five days. The maximum temperature was mostly occurred at the exterior ends of the bottom flange at thermocouples BF1 and BF9, while the

minimum temperature occurred at thermocouple BF8, which installed inside the box girder 0.5m from the interior face of the north web. On 29 May, the temperatures of the end thermocouples BF1 and BF9 were lower than those of the other thermocouples at 6:00 p.m. The sky was partially cloudy during the few hours before 6:00 p.m., which reduced the air temperature at this time. Thus, the outer ends were subjected to convection cooling instead of convection heating and solar radiation, which reduced the temperature of thermocouples BF1 and BF9 at this time.
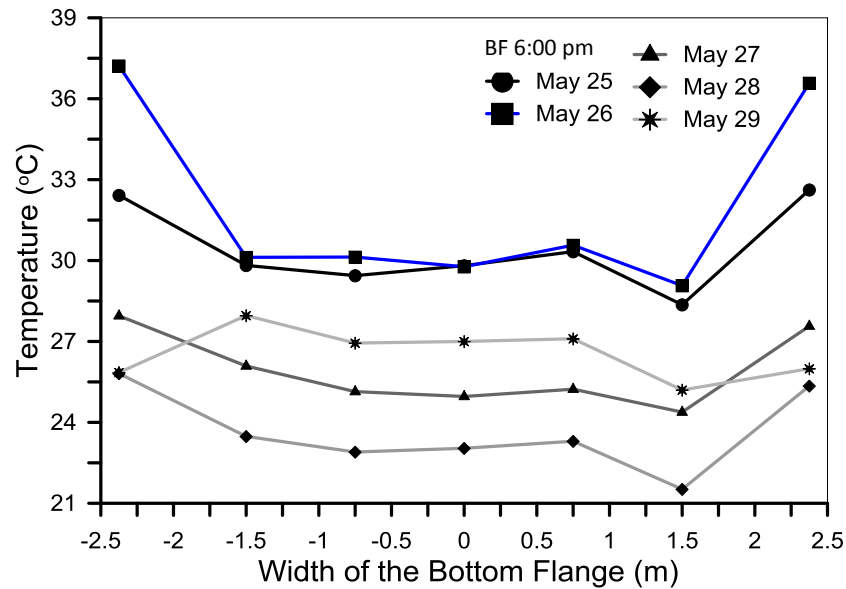

Figure 4.24 Temperature distributions along the bottom flange at 6:00 p.m.

Figure 4.25 shows the temperature distribution along the bottom flange at 3:00 a.m. during the five days. The effect of heat of hydration was explained in the previous section, the same results were found in Figure 4.25. The effect of heat of hydration was more important during the first 24 hours, decreased during the next 24 hours and almost negligible after about 100 hours.

It was illustrated at 26 May where the recorded temperature higher than the others, especially at the thermocouples BF1 and BF9 (at the exterior vertical faces), regardless of the low air temperature at this time (11.8 ℃.).

On 27 May and due to the low thermal conductivity of concrete and formwork, therefore the thermocouples BF1 and BF9 kept the residual heat of the previous

period, while the rest thermocouples at the same day recorded low uniform temperature compared with BF1 and BF9.

On 28 and 29 May the temperature distribution was slightly maximum at BF1 and BF9 than the others, because it affected by solar radiation and hot air during the daylight hours, and caused increase of the temperature, while the other thermocouples along the interior width of the bottom flange influenced by the shadow of the top slab. During the night hours it was started loss the temperature slowly, therefore the surface thermocouples as BF1 and BF9 was still recorded high temperature compared with the others at the same time.

At the 30 May and due to directly expose the thermocouples BF1 and BF9 to the low air temperature during the night hours (11.58 ℃) caused decreases in temperature recorded, while the temperature recorded at the other thermocouples was regular heat distribution because of it is located inside the cavity of the box girder. Table 4.6 shows the maximum and the minimum temperature distribution along the bottom flange of the concrete box girder segment.
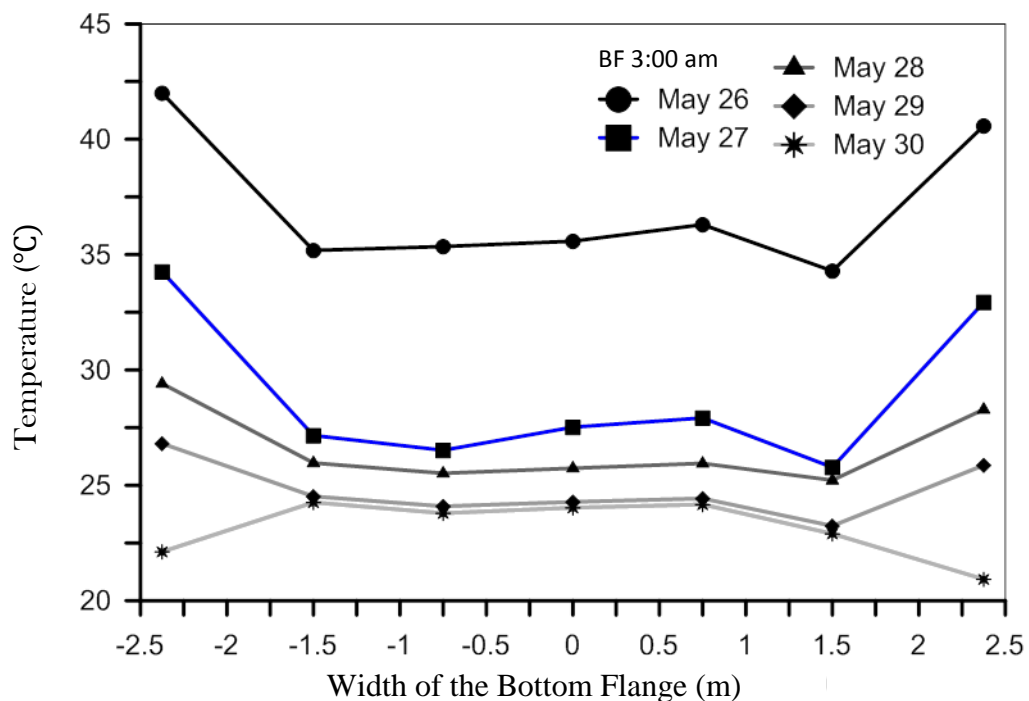
Figure 4.25 Temperature distribution along the bottom flange at 3:00 a.m.

Table 4.6 Maximum and minimum temperature distribution of bottom flange

No.thermocouple	Dates	Temperature (℃)	Air temperature (℃)
BF1	May 25 11:30 p.m.	43.21	13.99
BF9	May 30 6:00 am	19.55	12.75

4.6 Surface and Core Temperature Distributions during the First 12 Hours

Figure 4.26 shows the temperature distributions during the first 12 hours for thermocouples near the exterior surfaces, these thermocouples are TF6 (the top flange), BF6 (the bottom flange), SW9 (the south web), NW9 (the north web).

It is shown in Figure 4.26 that the temperature distributions of the four thermocouples were almost the same during the first six hours. Then after the temperature of all thermocouples has increased, however, the temperature of the thermocouples installed on the surfaces of the southern and northern webs increased in higher rates than the thermocouples installed on the surfaces of the top and the bottom flanges. This can be attributed to the different rates of cooling on the vertical and horizontal surfaces during the night hours. The convection cooling on the horizontal surfaces was higher than on the vertical surfaces (the webs) because the top and the bottom flanges were exposed to air from the top and sealed by formwork from the bottom, while both faces of the webs were sealed by formwork.

As shown in 4.26, the temperature of the top surface thermocouple TF6 of the top flange was lower than that of the bottom surface of the bottom flange BF6. This is simply because the top surface of the top flange is directly exposed to air, while the bottom surface of the bottom flange is sealed by formwork and is cooled slowly via the exposed top surface of the bottom flange

Table 4.7 shows the maximum temperatures in the first night during about 12 hours from the concrete pouring for exterior thermocouples TF6, BF6, SW9 and NW9, respectively
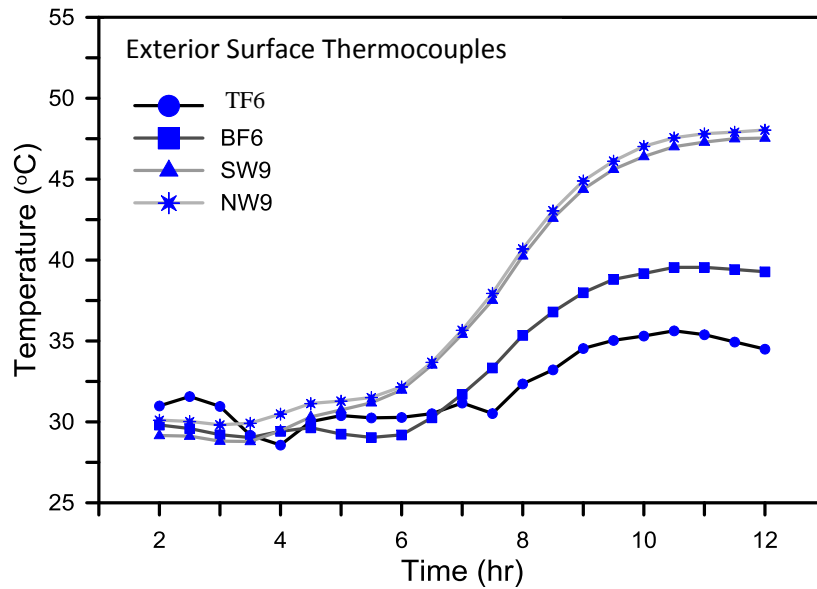
Figure 4.26 Temperature-time curves of the exterior surface thermocouples

Table 4.7 Maximum temperature distribution of exterior surface thermocouples

No.thermocouple	Dates	Temperature (℃)	Air temperature (℃)
TF6	May 25 10:00 p.m	35.63	15.63
BF6	May 25 10:00 p.m	39.55	15.63
SW9	May 25 11.30 p.m	47.54	14
NW9	May 25 11:30 p.m	48.04	14

Figure 4.27 shows the temperature distribution during the first 12 hours inside the box cavity at the centers of the interior faces, which are TF8 (the top slab), BF4 (the bottom slab), SW11 (the south web), and NW11 (the north web).

As for the exterior surface thermocouples, it is shown in the Figure 4.27 that the web thermocouples stilled showing higher temperatures compared with thermocouples TF8 and BF4. This is because the south and the north webs were covered by the formwork from both sides, while the top and the bottom flanges were exposed from the top surface and sealed from the bottom surface.

It is shown in Figure 4.27 that thermocouple TF8 at the lower sealed surface of the top flange showed close temperatures to those of the south and the north webs, while thermocouple BF4 which is exposed directly to the ambient air has recorded the lowest temperatures among the other four thermocouples because it is installed on

the top exposed surface of the bottom flange. Table 4.8 shows the maximum temperatures on the first night (during the first 12 hours) for the interior thermocouples TF8, BF4, SW11, and NW11, respectively

Figure 4.27 Temperature-time curves of the interior surface thermocouples

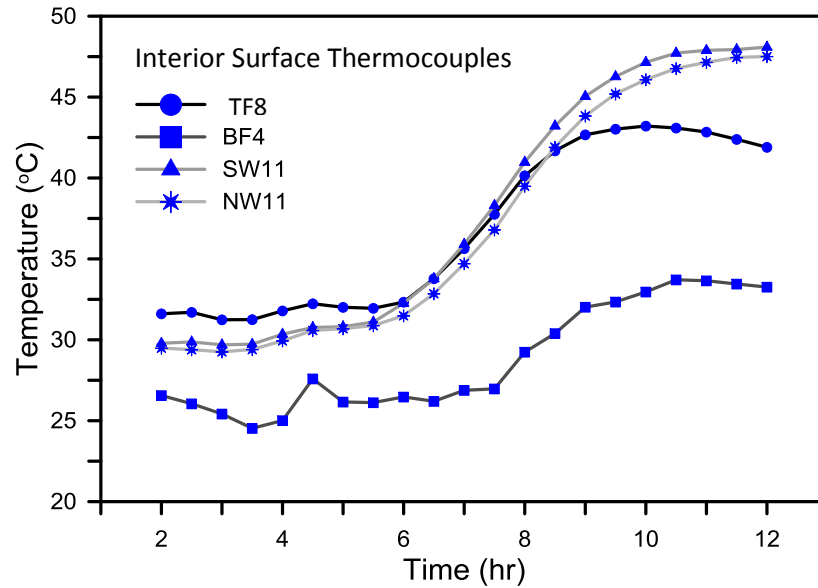**Table 4.8** Maximum temperature distribution of the interior thermocouples

No.thermocouple	Dates	Temperature (℃)	Air temperature (℃)
TF8	May 25 9:30 p.m.	43.21	16.14
BF4	May 25 10:00 p.m.	33.71	15.63
SW11	May 25 11.30 p.m.	48.1	14
NW11	May 25 11:30 p.m.	47.51	14

Figure 4.28 shows the temperature distribution during the first 12 hours for the core thermocouples that are installed in the centroids of the webs and flanges of the box-girder segment. These thermocouples are TS7 (the centroid of the top flange), BS5 (the centroid of the bottom slab), SW10 (the centroid of the southern web) and NW10 (the centroid of northern web).

The temperature distribution curves in Figure 4.28 validate the effect of sealing by formwork that discussed in Figure 4.26 and 4.27. The temperature of the webs, which were covered by the formwork from both sides were higher than the temperature of the top and bottom flanges, in which one surface was exposed to air

and one was sealed by formwork. Table 4.9 shows the maximum temperature distribution during the first 12 hours of core of concrete.

Figure 4.28 Temperature-time curves of the core thermocouples

Table 4.9 Maximum temperature distribution of the core thermocouples

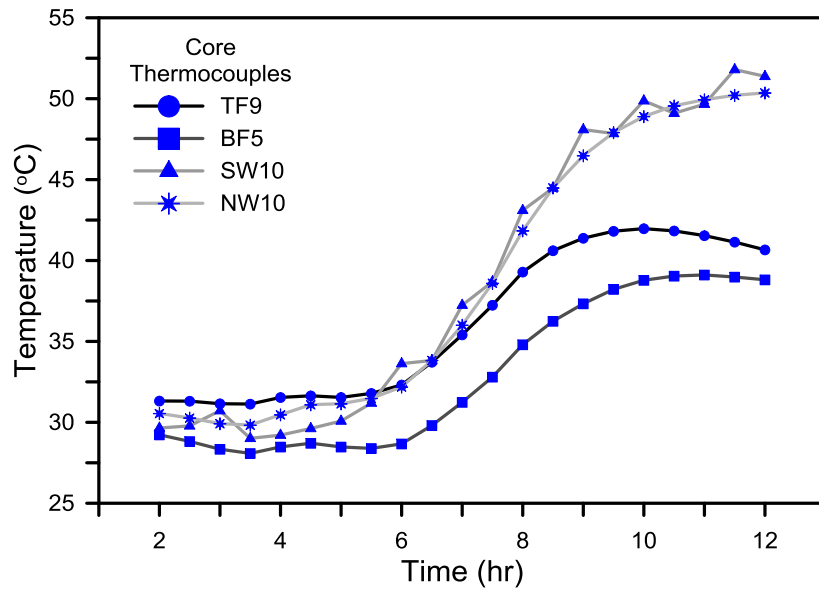| No.thermocouple	Dates	Temperature (℃)	Air temperature (℃)
TF7	May 25 9:30 p.m.	41.97	16.14
BF5	May 25 10:30 p.m.	39.11	15
SW10	May 25 11:00 p.m.	51.8	14.79
NW10	May 25 11:30 p.m.	50.36	14

4.7 Vertical Temperature Gradients

Figures 4.29 and 4.30 show the vertical temperature gradients at 1:00 p.m. of the first five days along the south and the north webs, which were presented along with the top flange thickness only (the top 200mm).

As discussed in the previous sections, the heat of hydration dominated the temperature distributions along the south web and the north web of box girder segment during the first 48 hours. It is shown in Figure 4.29 that the vertical temperature gradients at 1:00 p.m. on 25 and 26 May were negative. On the other hand, the vertical temperature gradients at the same time along the south and north webs on the following three days (27, 28, and 29 May) were positive with the

57

maximum temperature gradient at or near the top surface as shown in Figures 4.29 and 4.30.

Due to the high amount of heat released from the hydration of cement, the temperature of the interiors increased rapidly during the first 24 hours. The effect of solar radiation and air temperature during the hot hours of the day has raised the temperature of the top surface, however, its temperature was still less than the temperature of the concrete cores, which led to negative temperature gradient at 1:00 p.m. of the first day and the second day, i.e. during the first 24 hours from concrete casting. On the following days, the effect of hydration heat decreased due to the slow dissipation of this heat via the exposed surface, which reduced the interior temperature of the concrete and hence led to the normal behavior with positive gradient during the day hours.

The maximum vertical temperature gradient at the top surface of the top flange has increased with time because the effect of hydration heat was decreasing. The maximum negative temperature gradients at the top surface of south web at 1:00 p.m. on 25 and 26 May were 4.11 and 9.54 °C. On the other hand, the maximum positive temperature gradients at the top surface (south web at 1:00 p.m.) on 27, 28 and 29 May were 5.65, 10.15, and 16.46 °C, respectively as shown in Figure 4.29. The maximum temperature gradients at the top surface (north web at 1:00 p.m.) on 25, 26, 27, 28, and 29 May were 1.65, 4.39, 9.14, 13.61, and 14.09 °C, respectively as shown in Figure 4.30.
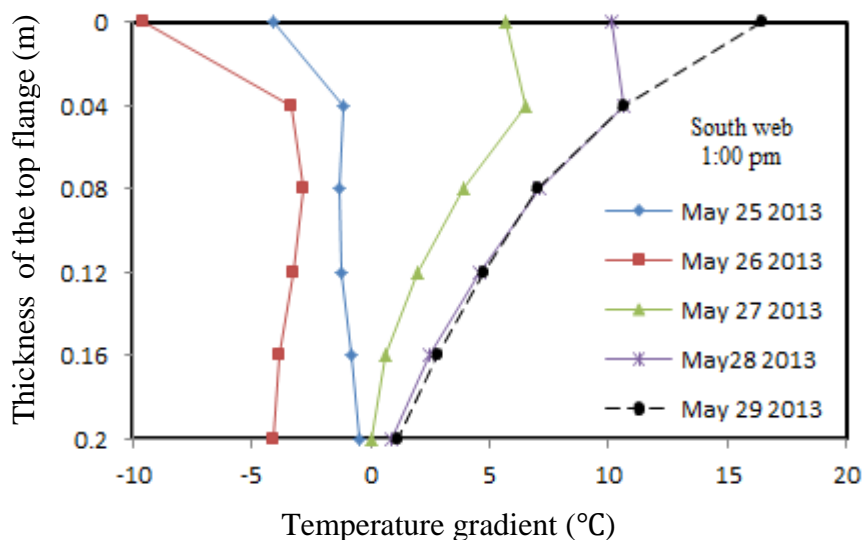
Figure 4.29 Vertical temperature gradient of south web along the top flange
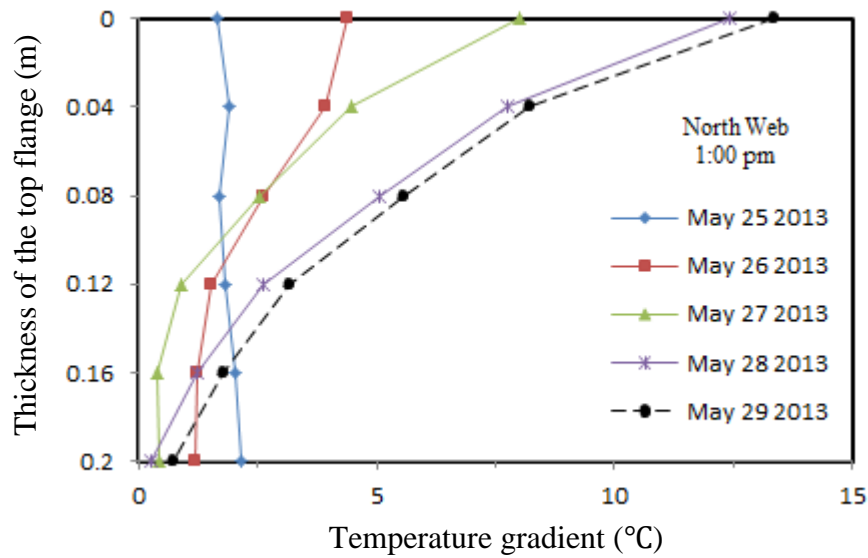
Figure 4.30 Vertical temperature gradient of north web along the top flange

The vertical temperature gradient along the south web during the five days are presented in Figure 4.31. As mentioned at the previous discussion the heat of hydration caused a rise in temperature of interior parts of concrete during the first 24 hours, thus as shown in Figure 4.31 the temperature gradients at 9:00 p.m. and 3:00 a.m. of the days 25 and 26 May were negative gradients during the daylight hours of 25 May and the night hours at the next day (26 May). Figure 4.31 illustrated the gradients at 9:00 p.m. and 3:00 a.m. of the 25 and 26 May were 22 and 23 ℃, the air temperature was about 16.4 ℃ and 11.38 ℃ respectively.

 During the following days, after about 48 hours of the cast of concrete, the influence hydration heat was a significant decrease. As shown in the figure the temperature gradient behavior was positive with a maximum in the near of the top slab due to high solar radiation at the horizontal surfaces. The temperature gradients at 3:00 p.m. of the 27 and 29 May were 5.6 ℃ and 7.44 ℃ respectively, the air temperature was about 28 and 29 ℃ of the previous two days.
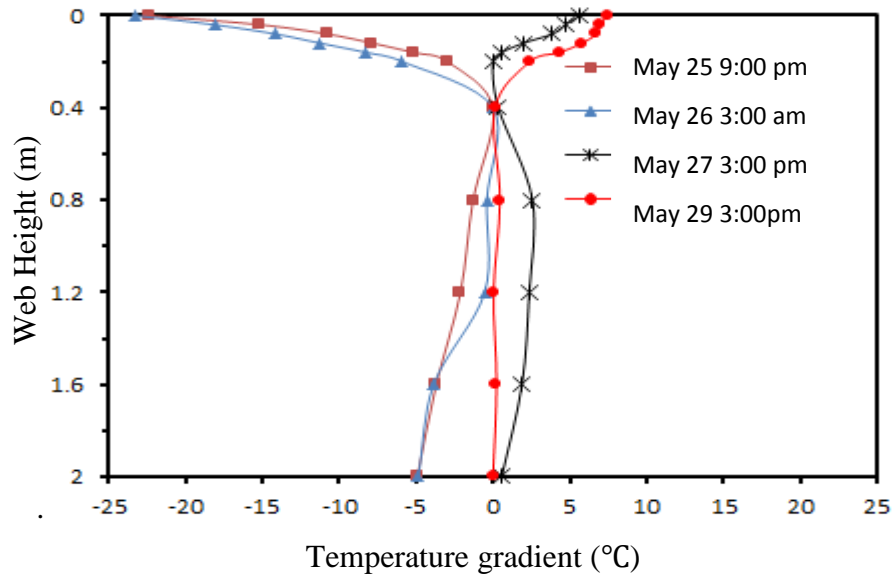
Figure 4.31 Vertical temperature gradient of the south web

Figure 4.32 shows the vertical temperature gradient of the north web during five days of the concrete box girder, a similar sequence of results can be shown in Figure 4.32 . The negative gradient occurred at 9:00 p.m. and 12:00 a.m. (at the midnight) of the 25, 26 May, where the temperature gradients were about 15.5 ℃ and 17.24 ℃ respectively. The following days, the hydration heat was decreased and the temperature gradients were positive with a maximum at the top surface, the temperature gradients were recorded in the north web on 27, 29 May were 5 ℃ and 8 ℃ respectively at 3:00 p.m., the air temperature 28 and 29 ℃ at this time.
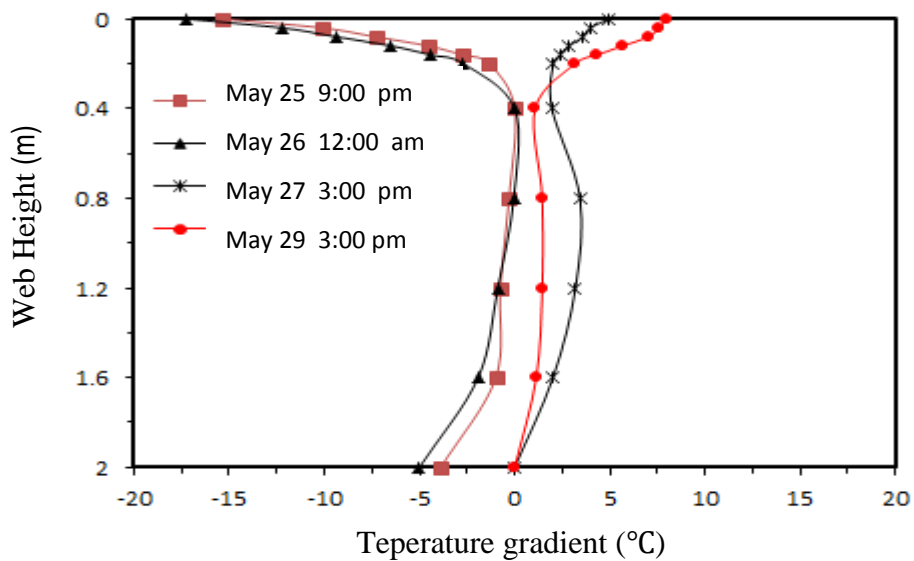

Figure 4.32 Vertical temperature gradient of the north web

4.8 Transverse Temperature Gradient

Figure 4.33 shows the negative transverse thermal gradient along the mid thickness of the top flange at 3:00 a.m. of the day 26 May from the Figure it can be seen that the value of temperature gradient was 9.1 ℃ at TF1 in the vertical face of southern edge, while the value was zero occurred at TF10. The negative thermal gradient at the northern edge was 7.28 ℃. At 12:00 a.m. of the day 27 May the negative thermal gradient at TF1 southern end of the top slab was 5.67 ℃.

While the negative thermal gradient was zero at TF10, in which located 2.125 m from the northern edge of the top flange of the box girder. The negative thermal gradient at the northern end of the top flange was 4.85 ℃. From observation of the Figure it can be seen that the temperature gradients at 27 May, less than the 26 May because of reduction the effect of the hydration heat with time.
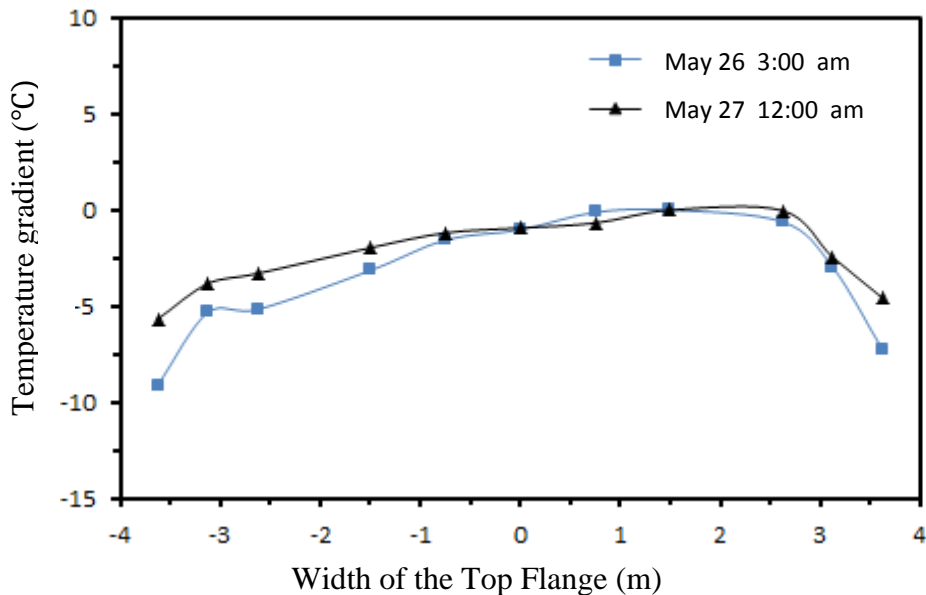
Figure 4.33 The negative thermal gradient along the top flange

Figure 4.34 shows the positive transverse thermal gradient along of the mid thickness of the top flange. At 3:00 p.m. on 27 May, the positive thermal gradient at TF1 with a value of 2.06 ℃ then increased to 3.53 ℃ at TF3 which located 1.0 m from the southern edge of the top flange, the gradients at the rest length of the top flange was uniform to TF11, then increased to 1.39 ℃. From Figure 4.34 it can be seen that the thermal gradients at the southern edge almost higher than the northern edge due to the orientation of the box girder (East- West).

61

From the Figure, the thermocouples TF1 and TF13 (at the external ends) recorded thermal gradients more than the interior thermocouples because it affected by solar radiation compared the others. At 3:00 p.m. of 29 May as same behavior of 27 May .

At 11:30 a.m. of the 30 May (after 120 hours of the concrete pouring), it can be seen that the jump at thermocouple TF1 (6.64 ℃), because the intensity of solar radiation at the southern side of the box girder at this time.
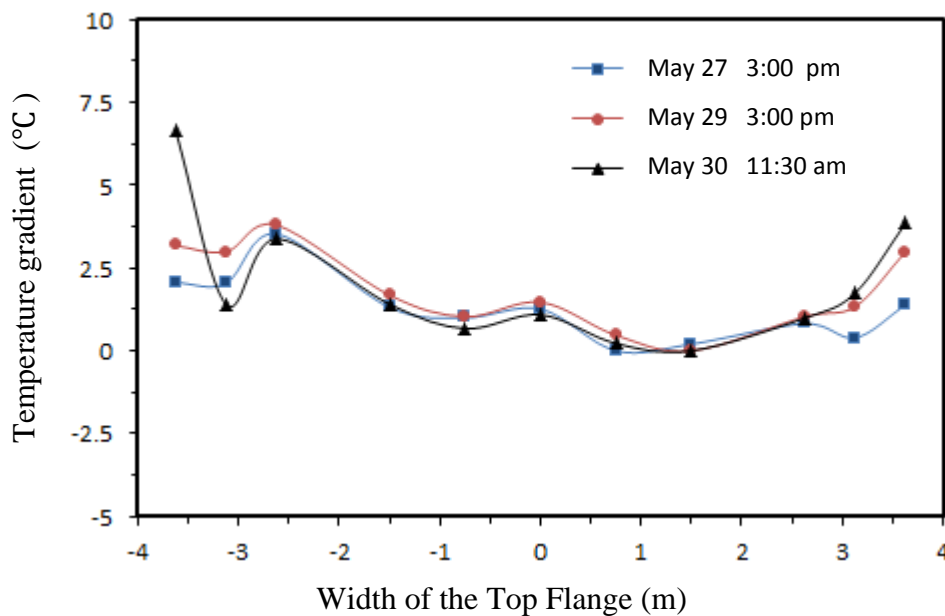

Figure 4.34 The positive thermal gradient along the top flange

Figure 4.35 shows the negative transverse thermal gradients along the bottom flange at different time steps. From the Figure, it can be seen that the value of the negative gradients at 6:00 p.m. of the 29 May was zero at BF2 (0.875 m from the southern edge) and to 2.11 ℃ at BF1, while the negative gradient was 1.97 ℃ at BF9 (the northern edge).

The thermal gradients at the edges of the bottom flange less than the rest thermocouples at the interior length, while the other thermocouples recorded uniform values, because it was directly subjected to the cooling by convection process, where the air temperature begun trending to decline due to sunset at this time. At 3:00 a.m. of the 30 May (after 112 hours from concrete pouring), the negative transverse thermal gradient seen to follow the thermal gradient of 29 May

excepting at the northern edge (at the thermocouple BF9), which affected by convection cooling at night where, the air temperature 11.05 ℃ at this time.
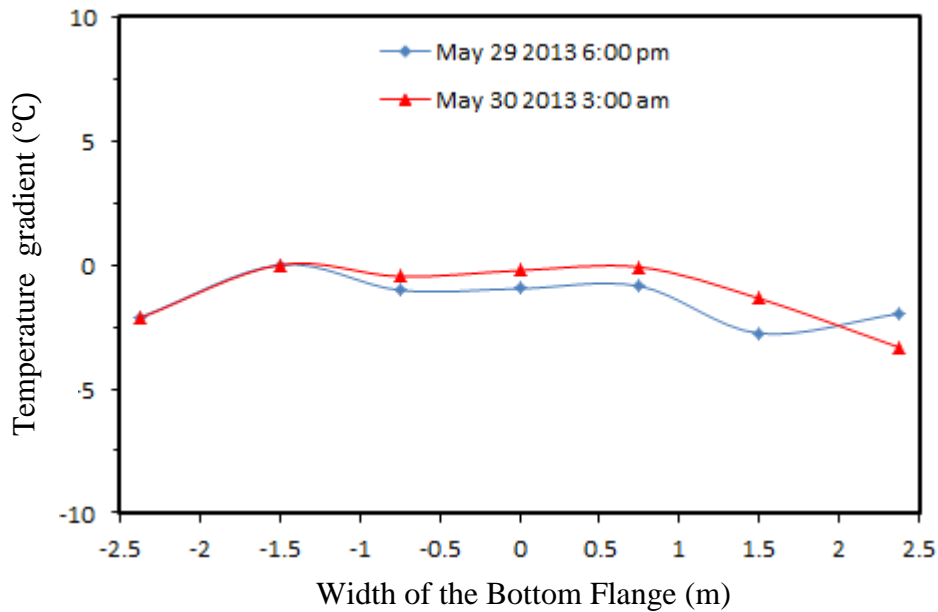

Figure 4.35 The negative thermal gradient along the bottom flange

Figure 4.36 shows the positive transverse thermal gradient in the bottom flange from Figure 4.36 it can be seen that the maximum values at 1:00 p.m. of the 27, 28, and 29 May occurred at the southern edge of the bottom flange because affected by solar radiation and hot air at the edges of the box girder and the thermal gradients at the southern higher than the northern edge, because and as mentioned in the previous section due to the orientation of the box girder (East- West).

The thermal gradient at thermocouples of the interior length were uniform and less than the thermocouples BF1 and BF9, due to the effect of the shadow of the top flange, and it gained heat by conduction process through the thickness of the bottom flange. The maximum temperature gradients of the 27, 28, and 29 May at the southern edge of the box girder were 5.02, 2.89, and 1.7 ℃ respectively.
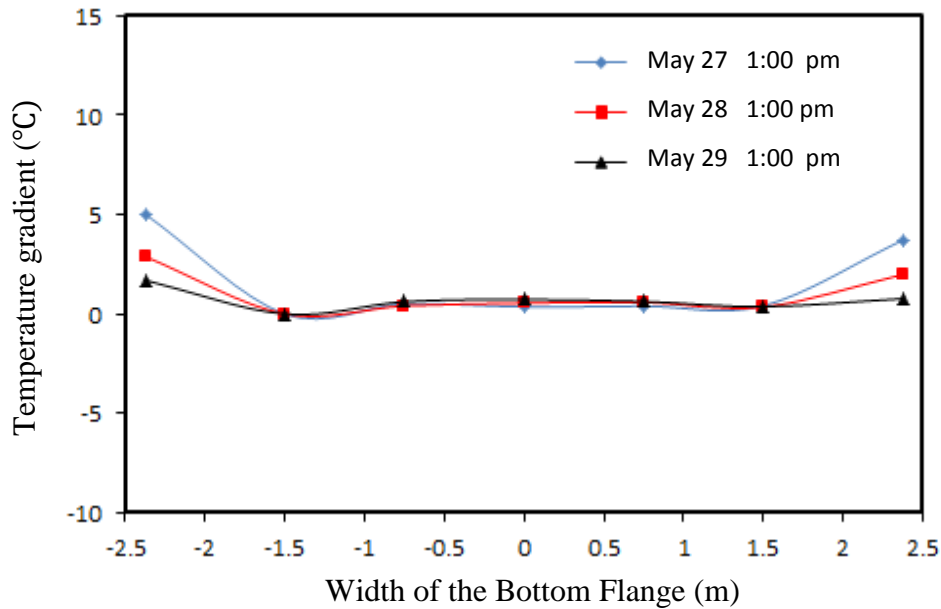
Figure 4.36 The positive thermal gradient along the bottom flange

4.9 Comparison with the AASHTO LRFD Design Specifications 2012

For the concrete box girder segment, the positive thermal gradient was plotted in Figure 4.37 and it was compared with the recommended positive gradient of the AASHTO LRFD Code 2012 zone 4, the measured thermal gradient along the south and north webs of 16.21 ℃ and 11.6. ℃ at 1:30 p.m. and 2:00 p.m. on 29 May respectively. The design gradient of the AASHTO LRFD 2012 zone 4 was 21 ℃, as shown Figure 4.37 the measured thermal gradients were almost smaller than the design gradient of AASHTO code.

As mentioned in the chapter one, this study conducted at the end of spring (beginning the summer) and limited for several days. Presumably with more data (as high intensity of solar radiation and increase ambient air temperature), thus the measured value of maximum thermal gradient would be increased, and the difference between the design gradient of AASHTO and the measured thermal gradient of 29 May in the webs in Figure 4.37 would be minimized.
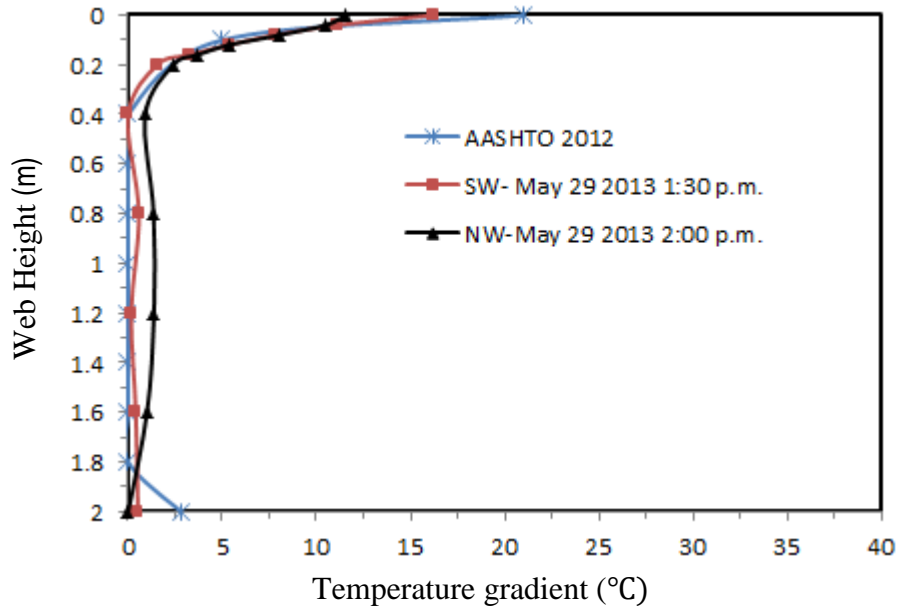
Figure 4.37 Comparisons between the positive thermal gradient along the south and the north webs with the design gradient of AASHTO code

Figure 4.38 shows the comparison between the recommended negative design gradient of the AASHTO LRFD 2012 and the negative thermal gradients along the south and north webs, as shown Figure 4.38, at the first day (after about 12 hours from the concrete pouring), where the effect of heat of hydration at the early age of concrete, thus the soffit of concrete is much hotter than the top surface, so the value of negative thermal gradient(at the first 12 hours) was higher than the negative design gradient of AASHTO 2012.

The AASHTO LRFD specifications does not take into account the early age of concrete for the design thermal gradient, and be taken into account the maximum environmental conditions for long periods in determining the design gradients.

At 6:00 a.m. of the 29 May and after about 100 hours the influence of hydration heat almost negligible and the maximum negative thermal gradient occurs during at the early morning due to convection cooling at the top surface, while the soffit of concrete still warmer, because the low thermal conductivity of concrete. The value of negative thermal gradients of the south and the north webs were 6.77 ℃ and 6.24 ℃ respectively.
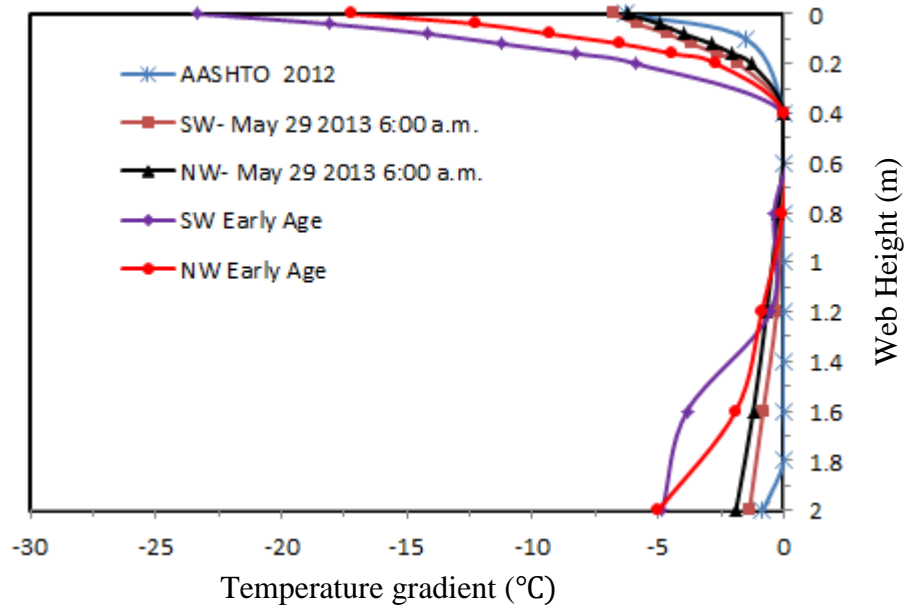
Figure 4.38 Comparison between the negative thermal gradient along the south and north webs with the design gradient of AASHTO code

CHAPTER 5

CONCLUSIONS

5.1 Conclusion

Temperature measurements from an experimental study with a reinforced concrete box girder segment using 48 thermocouples were utilized in this research to investigate the temperature distributions and gradients along the webs and the flanges of concrete box girder bridges during the early age of concrete. From the results of the current study, several conclusions were obtained:

1- The heat of hydration of concrete has a significant effect on the temperature distribution of concrete box girder bridges during the early age. After 48 hours, the effect of hydration heat decreased and was almost negligible after four to five days.

2- The temperature distribution during early age was affected by the heat of hydration and the environmental condition such as solar radiation and air temperature. The degree of the effect of heat of hydration depends mainly upon the location of thermocouples, the volume of concrete, which surrounded the thermocouples and the degree of sealant by formwork.

For the thermocouples that were installed near an exposed surface, the environmental thermal loads affect the temperature –time curves more than the heat of hydration. The heat of hydration behavior was controlled for thermocouples which were installed away from the exposed surface or those covered by formwork from both sides. The thermocouples SW7 and NW7 were located of the flange-web junction showed higher temperatures and were completely controlled by the heat of hydration during the first 48 hours. The surface thermocouples SW1and NW1 showed lower dependency on heat of hydration and almost followed the air temperature behavior during the early hours of the concrete age.

3- The fluctuation of solar radiation reflects the state of the cloud cover during the five days and although the first two (days 25 and 26 May) were partially cloudy, the maximum difference between surfaces and interior parts of the segment were recorded after the mid of the first night (after about 12 hours). At this time, the surface was gradually cooled because the air convection (at night) affecting on the temperature of the top surface of concrete, while the temperature at the cores of concrete reached to the peak due to the liberated heat from cement hydration. The maximum temperature gradient along the south web at 2:00 a.m. on the first night was about 25 ℃.

4- The temperature of the top concrete surface of the aged concrete should be more than the other parts during the midday hours, but in the current study, the temperature of the top surface was lower than the interior parts of the concrete. This result was due to the magnitude of hydration heat liberated during the first 24 hours. The heat of hydration increased the temperature of the interior parts of the concrete and it remains the highest during the first day (about 24 hours) in spite of the top surface heating by solar radiation. When the effect heat of hydration gradually reduced with time, the behavior of concrete changed to be the behavior of hardening concrete.

5- The maximum lateral temperature distribution on the top surface always occurs near the thermocouples at the top flange-web junction, which were surrounded with the highest concrete volume among the others. The orientation of the box girder segment (East- West) and the seasonal condition (end of spring) caused the production of higher temperature at the south web than the north during the day hours of all days.

6- Along the bottom flange, the maximum temperature occurred at the outer ends, while the temperature was almost uniform along the rest length.

7- The measured thermal gradients were comparison with the AASHTO LRFD Design Specifications 2012.

REFERENCES

[1] National Concrete Pavement Technology Center. January (2006). Final Report for developing a simple and rapid test for heat evolution of concrete, pp. 38.

[2] Lerch, W. and Ford, C.L. (1948) Long time study of cement performance in concrete Chapter 3: Chemical and physical test of the cement, *ACI Journal, Proceeding*, **44**, (8), pp. 743- 795.

[3] Danish Concrete Association. (1990). Recommendations for curing concrete, Denmark, pp. 27.

[4] Lerch, W. Bogue, R. H. (1934). Heat of hydration of portland cement pastes. *Journal of Research of National Bureau Standards.* **12,** pp. 645-664.

[5] Lerch, W. (1946). The influence of gypsum on the hydration and properties of Portland cement pastes. *Proceedings of American Society for Testing Materials* **46**, pp. 1252-1297.

[6] Qian, Z. Schlangen, E. Breugel, K. (2010). 3D Simulation of the micromechanical behavior of cement paste. Microlab, Delft University of Technology, the Netherlands.

[7] ASTM C 494. Standard Specification for Chemical Admixtures for Concrete.

[8] ASTM C 186. Standard Test Method for Heat of Hydration of Hydraulic Cement.

[9] Holman, J. (1986). Heat Transfer, 6th Ed. McGraw – Hill book company, New York, pp. 676.

[10] Kriith, F. (1973). Principles of heat transfer, 3rd Edition, Intex Educational Publishers, New York, pp. 620.

[11] Duffie, J. A. and Beckman, W. A. (1974). Solar energy, thermal processes, John Wily and Sons, Inc. pp. 386.

[12] Billington, N. S. (1952). Thermal properties of building, Cleaver- Hume Press, London, pp. 209.

[13] Emerson, M. (1976). Bridge temperatures estimated from the shade temperature, Report LR 696, Transport and road laboratory, Crowthorne, pp. 21.

[14] Hulsey, J. L. (1976). Environmental effects on composite girder bridge structures PhD Dissertation, Dep. Of civil engineering, University of Missouri – Rolla, USA, pp. 265.

[15] Dilger, W. H. and Ghali, A. (1980). Temperature induced stresses in composite box-girder bridges, a research report by Dilger- Ghali civil

engineering consulting Ltd., submitted to the Department of supplies and services, Canada, pp. 179.

[16] Zuk, W. (1961). Thermal and Shrinkage Stresses in Composite Beams. *ACI Journal*, **58** (3), pp. 327-340.

[17] Zuk, W. (1965). Thermal Behavior of Composite Bridges-Insulated and Uninsulated, Highway Research Record 76, National Research Council, pp. 231-253.

[18] Emerson, M. (1968). Bridge temperature movements in the British Isles. TRRL Report, No LR 288, Transport and Road Research Laboratory, England.

[19] Maher, D. R. H. (1970). The effects of differential temperature on continuous prestressed concrete bridges. Civil Engineering Transactions Institution Engineers, Australia, **12** (273), CE12, No 1. pp. 29-32.

[20] Emerson, M. (1973). The calculation of the distribution of temperature in bridge (TRRL Report LR 561). Berkshire, UK: Transport and Road Research Laboratory.

[21] Will, K. M. Johnson, C. P. and Matlock, H. (1977). Analytical and experimental investigation of the thermal response of highway bridges (Research Project 23-2). Interim report to Texas state department of highways and public transportation, University of Texas at Austin.

[22] Priestly, M. J. N. (1976). Design Thermal Gradients for Concrete Bridges, *New Zealand Engineering*, **31** (9), pp. 213-219

[23] Degenkolb, O. H. (1977) . Concrete Box Girder Bridges. American Concrete Institute (ACI).

[24] Hambly, E. C. (1978). Temperature distribution and stresses in concrete bridges. The Structural Engineer, **56,** pp. 143 - 148.

[25] Emanuel, J. H. and Hulsey, J. L. (1978). Temperature distributions in composite bridges, *Journal of the Structural Division*. ASCE, **104**, pp. 65-78.

[26] Wood, J. H. (1979).   Thermal measurements of ambient thermal response of concrete bridges. RRU Bulletin 42, National Road Research Board, New Zeland State Highways, Wellington.

[27] Wanders, S. P. (1979). Study of the segmental box girder bridge at Turkey Run. Construction, Instrumentation and Data Collection, School of Engineering, Purdue University, Indiana, USA, Report No FHWA / IN / JHRP, pp. 147.

[28] Dilger, W. H. Ghali, A. and Cheung, M. S. (1981). Field measurements of Muskwa River bridge. *Journal of Structural Division*, **107**, pp. 2147-2161.

[29] Hoffman, P. C. Claure, R. M. and West, H. H. (1983). Temperature Study of an Experimental Segmental Bridge. PCI Journal, **28**, pp.78-79.

[30] Elbadry, M. M. and Ghali, A. (1983). Temperature variations in concrete bridges, *Journal of Structural Engineering*, ASCE, **109**, pp. 2355-2374.

[31] Elbadry, M. and Ghali, A. (1986). Thermal stresses and cracking of the concrete bridges, *ACI Journal*, **83**, pp. 1001-1009.

[32] Mirambell, E. and Aguado, A. (1990). Temperature and stress distributions in concrete box girder bridges. *Journal of Structural Engineering*, **116**, pp. 2388- 2409.

[33] Moorty, S. and Roeder, C. W. (1992, April). Temperature-dependent bridge movements. *Journal of Structural Engineering*, **118**, pp. 1090-1105.

[34] Gilland, J. A. and Dilger, W. H. (1997). Monitoring concrete temperature during construction of the confederation bridge. *Canadian Journal of Civil Engineering*, **24**, pp. 941-950.

[35] Roberts, C.L. Breen, J.E. and Cawrse, J. (2002). Measurements of thermal gradients and their effects on segmental concrete bridge. *Journal of Bridge Engineering*, **7**, pp. 166-174.

[36] Pisani, M. A. (2004, August). Non-linear strain distributions due to temperature effects in compact cross-sections. *Engineering Structures*, **26**, pp. 1349-1363.

[37] Zhang, L. Wu, L. and Yang, L. (2012). Analysis of temperature field of concrete box girder and secondary development of program, *Journal of Convergence Information Technology*, **7**.

[38] AASHTO. (2012). LRFD Bridge Design Specifications. 4th Ed. American Association of State Highway and Transportation Officials. USA, Washington, D.C.

[39] GU, Bin. Chen, Zhi. and Chen, Xin. (2014). Temperature gradients in a concrete box girder under the effect of the cold wave. J. Cent. Univ. pp. 1227-1241.

[40] AASHTO. (1989). AASHTO Guide Specifications thermal effects in concrete bridge superstructures. American Association of State Highway and Transportation Officials. USA, Washington, D.C.

[41] AASHTO. (2010). AASHTO LRFD Bridge Design Specifications, 4th Ed. American Association of State Highway and Transportation Officials (AASHTO). USA, Washington, D.C.

[42] DINI. 072. (1967). Road and Foot Bridges Design Loads, Deutsche institute Normung, Berlin.

[43] Abid, S. R. (2013). Ph.D Second Progress Report. University of Gaziantep, Department of Civil Engineering.